Climate signal propagation in southern California aquifers

Janet Barco,[1] Terri S. Hogue,[1] Manuela Girotto,[1] Donald R. Kendall,[2] and Mario Putti[3]

Received 9 July 2009; revised 4 July 2010; accepted 10 August 2010; published 23 November 2010.

[1] The western United States is marked by limited water resources and a fast-growing population. Increasing climate variability as well as a growing demand on water resources highlights the need for improved understanding of connections between regional climate, surface water dynamics, and groundwater recharge. The current study focuses on the linkages between climate variability and groundwater levels in Calleguas Creek watershed located in southern California. The Calleguas Creek groundwater system serves as a critical source of water supply for agricultural and industrial use. Precipitation time series and groundwater levels were analyzed throughout the Calleguas Creek watershed for the period 1975–2004. Water level variability was analyzed for over 311 individual wells with a subset of 20 wells selected for further analysis. A correlation matrix was computed to establish well locations (or groups) with similar hydrologic behavior. Prewhitening methods were used to evaluate the effect of time series autocorrelation on the test statistics for trend detection using the Mann-Kendall test. Both climate and selected groundwater level (well) data were subjected to frequency analysis using fast Fourier transform. The time series of precipitation, the El Niño–Southern Oscillation (ENSO) index, and well levels were analyzed. A strong persistence was observed in the groundwater level time series, ranging from 66% to 99%. Results suggest the existence of significant periodicities between 2.0 and 7.0 years in both the precipitation and the well level data that are partially coincident with ENSO modes. A decadal oscillation was also observed in the well level data, which partially corresponds with the Pacific Decadal Oscillation. Assessment of the complex interactions between climate variability and groundwater levels will facilitate improved water resources planning and management in water-stressed regions where marginal changes in hydrologic budgets have significant implications.

Citation: Barco, J., T. S. Hogue, M. Girotto, D. R. Kendall, and M. Putti (2010), Climate signal propagation in southern California aquifers, *Water Resour. Res.*, *46*, W00F05, doi:10.1029/2009WR008376.

1. Introduction

[2] Groundwater is an essential component of global and regional water supply. Worldwide, one quarter of the population is dependent on groundwater for drinking water [*Glennon*, 2002] with many regions practicing unsustainable groundwater use [*Burke and Moench*, 2000; *Gleick*, 2003; *Ahmadi and Sedghamiz*, 2007]. In the United States, groundwater constitutes more than 25 percent of the supply for domestic purposes and is considered a principal reserve of freshwater for future water supply [*Alley et al.*, 1999]. Improved understanding of the variability in groundwater inflows and outflows, and the potential impact on changes in short-term and long-term storage, is essential for water resources planning and management, particularly in arid and semiarid regions [*Hogan et al.*, 2004; *Scanlon et al.*, 2006].

[3] California experiences significant groundwater withdrawals, accounting for 18% of the total groundwater withdrawal across the United States [*Hutson et al.*, 2004]. In southern California, nearly 40% of the regional water supply is obtained from groundwater [*California Department of Water Resources* (*CDWR*), 2003]. Because of its semiarid climate, much of California has extensive regions of developed agriculture that are highly dependent on irrigation to meet crop water demands over the growing season [*CDWR*, 2003]. Unfortunately, the increasing amount of water necessary for a rapidly growing population (Southern California Association of Governments, http://www.scag.ca.gov/census/index.htm) and widespread agriculture has created extensive overdraft conditions in groundwater systems throughout the state [*Stamos et al.*, 2001; *CDWR*, 2003; *Hanson and Dettinger*, 2005; *Faunt*, 2009]. Overdraft not only affects aquifer water levels but also significantly impacts connected surface flows and ultimately, riparian habitat [*Lines*, 1996; *Lines and Bilhorn*, 1996]. Furthermore, as urban (impervious cover) areas increase, groundwater levels generally decrease as a result of the combined effects of groundwater pumping and loss of groundwater recharge [*Hoque et al.*, 2007]. When groundwater systems are approaching or exceeding their limits of sustainability, even small changes in recharge, outflow, or storage may have economic or environmental consequences [*Mayer and Congdon*, 2008]. More effective

[1]Department of Civil and Environmental Engineering, University of California, Los Angeles, California, USA.
[2]Calleguas Municipal Water District, Thousand Oaks, California, USA.
[3]Department of Mathematical Methods and Models for Scientific Applications, University of Padua, Padua, Italy.

0043-1397/10/2009WR008376

management practices are being sought to ensure the future availability and reliability of groundwater resources and this effort can benefit from a better understanding of the links between cyclical signals in regional climate and corresponding groundwater response.

[4] Modeling the impact of climate change and associated variability on hydrology has been the center of much attention for several decades [*Gleick*, 1985; *Dracup and Kendall*, 1989; *Nash and Gleick*, 1993; *Hamlet and Lettenmaier*, 1999, *Christensen et al.*, 2004]. Several studies illustrate linkages between hydrology and climate quasiperiodic modes in the southwestern United States [*Rasmussen*, 1984; *Andrade and Sellers*, 1988; *Cayan et al.*, 1999; *Simpson and Colodner*, 1999; *Hanson et al.*, 2004, 2006; *Thomas*, 2007, *Mayer and Congdon*, 2008], including El Niño–Southern Oscillation (ENSO), Pacific Decadal Oscillation (PDO) and Atlantic Multidecadal Oscillation (AMO). ENSO is associated with some of the most pronounced interannual climate variation in the southern California region [*Dettinger et al.*, 1998; *Voisin et al.*, 2006; *Guirguis and Avissar*, 2008; *Intergovernmental Panel on Climate Change* (*IPCC*), 2001]. ENSO is known to have significant economic, environmental, and social impacts around the globe [*Mantua et al.*, 1997; *Trenberth and Karon*, 2000, *IPCC*, 2001; *Glantz*, 2001; *Poveda et al.*, 2001; *Bove*, 1998]. The PDO has been described as a long-lived ENSO-like pattern of Pacific climate variability [*Zhang et al.*, 1997], and is also connected to streamflow and drought anomalies in western North America [*Cayan*, 1996, *Mantua et al.*, 1997; *Hamlet and Lettenmaier*, 1999; *Nigam et al.*, 1999]. Positive PDO is related to higher precipitation in the southwest, while conditions reverse during negative PDO phases [*MacDonald and Case*, 2005]. A characteristic that distinguishes the PDO from ENSO is that PDO episodes have shown remarkable persistence relative to that attributed to ENSO events [*Mantua et al.*, 1997; *Minobe*, 1997]. Interdecadal variations on the order of 10–25 years may be related to the PDO [*Mantua and Steven*, 2002]. Previous studies have noted a 10 year cycle in groundwater level fluctuations associated with PDO [*Hanson et al.*, 2004; *Gurdak et al.*, 2007].

[5] Climatic periodicity in hydrology has been identified empirically from cross correlation and moving averages [*Chen et al.*, 2004; *Mayer and Congdon*, 2008]. Alternatively, periodicity can be estimated directly from time series using singular spectrum analysis [*Hanson et al.*, 2004; 2006; *García et al.*, 2005; *Gurdak et al.*, 2007], Fast Fourier transform methods [*Fraedrich and Boettger*, 1978; *Mann and Park*, 1994; *Diaz and Pulwarty*, 1994; *Venencio and Garcia*, 1998; *Morales and Poveda*, 2009] or wavelet analysis [*Torrence and Compo*, 1998; *Labat et al.*, 2004; *Kang and Lin*, 2007; *Zhang et al.*, 2007]. Many past studies on groundwater flow in the southwestern United States have generally neglected climate variability and the relationship to aquifer fluctuations [*Hanson et al.*, 2003, 2004; *Mayer and Congdon*, 2008]. Furthermore, anthropogenic effects may be on the scale of natural climate variability, confounding analysis and making it difficult to distinguish between the two signals [*Mayer and Congdon*, 2008].

[6] There are few published studies evaluating temporal and spatial fluctuations in groundwater levels in the western United States. *Hanson et al.* [2004] proposed a method for the frequency analysis of hydrologic time series. To demonstrate application of the method, hydrologic time series from the Mojave River Basin, California, were analyzed. Results showed that climatic variability exists in precipitation, streamflow and groundwater levels and that the variability is partially coincident with the Pacific Decadal Oscillation (PDO) and El Niño–Southern Oscillation (ENSO). Using the same methodology of *Hanson et al.* [2004]), a follow-up paper [*Hanson et al.*, 2006] analyzed hydrologic time series for two alluvial basins located in southern California and two located in southeastern Arizona. The study focused on demonstrating the connections between climate indices (PDO, ENSO and North American Monsoon, NAM) and hydrologic time series (precipitation, streamflow, tree ring indices and groundwater levels). The study revealed that PDO is the largest contributor to cyclic hydrologic variability for all basins. Stronger time series variation associated with PDO and ENSO was identified in the California basins, while the Arizona time series exhibited more variation linked with NAM. The Southern California basins included the Santa Clara–Calleguas groundwater basin. Using cluster analysis and time series seasonal decomposition, *Mayer and Congdon* [2008] studied climate and pumping signals in a groundwater system located in the southwestern United States. They showed that both climate and pumping impacts are propagated at approximately the same scale throughout much of the flow system.

[7] In the current study, we undertake a time series analysis of hydroclimatic data in a southern California watershed that is heavily dependent on its groundwater supply. Our primary goal is to illustrate linkages between ENSO modes, precipitation variability and aquifer response. Water level variability is analyzed for 20 wells, seven precipitation gages and the El Niño–Southern Oscillation (ENSO) index. We also explore the relation between the Pacific Decadal Oscillation (PDO) and groundwater variability. The wells selected in our study cover a range of elevations (18–330 m) and geologic formations; both upper and lower aquifers were included with depths ranging from 28 m to 564 m and covering both confined and unconfined aquifers. Correlation analysis was used to establish well groups with similar hydrologic behavior. A prewhitening technique was used to evaluate the effect of time series autocorrelation on the test statistics for trend detection. A nonparametric trend analysis was applied to account for long-term behavior in the studied series. Hydrologic periodicities were also evaluated using fast Fourier transform.

2. Data and Methods

2.1. Study Area

[8] The Calleguas Creek watershed, located northwest of metropolitan Los Angeles, is 878 km^2 and runs primarily from east to west, draining into the Pacific Ocean through Mugu Lagoon (Figure 1). The basin is bounded on the north by the Santa Susana Mountains, Oak Ridge, and South Mountain, and on the south by the Simi Hills and Santa Monica Mountains. Oak Ridge separates Calleguas Creek Watershed from that of the Santa Clara River to the north. Land use varies throughout the watershed, with approximately 25% urban, 25% agriculture, and 50% undeveloped land cover [*Calleguas Creek Watershed Management Plan Committee* (*CCWMP*), 2004]. Agricultural land is dominated by orchards of lemons and avocados, and field of strawberries, celery and tomatoes (CCWMP, personal communication, 2004). The headwaters of Calleguas Creek originate in

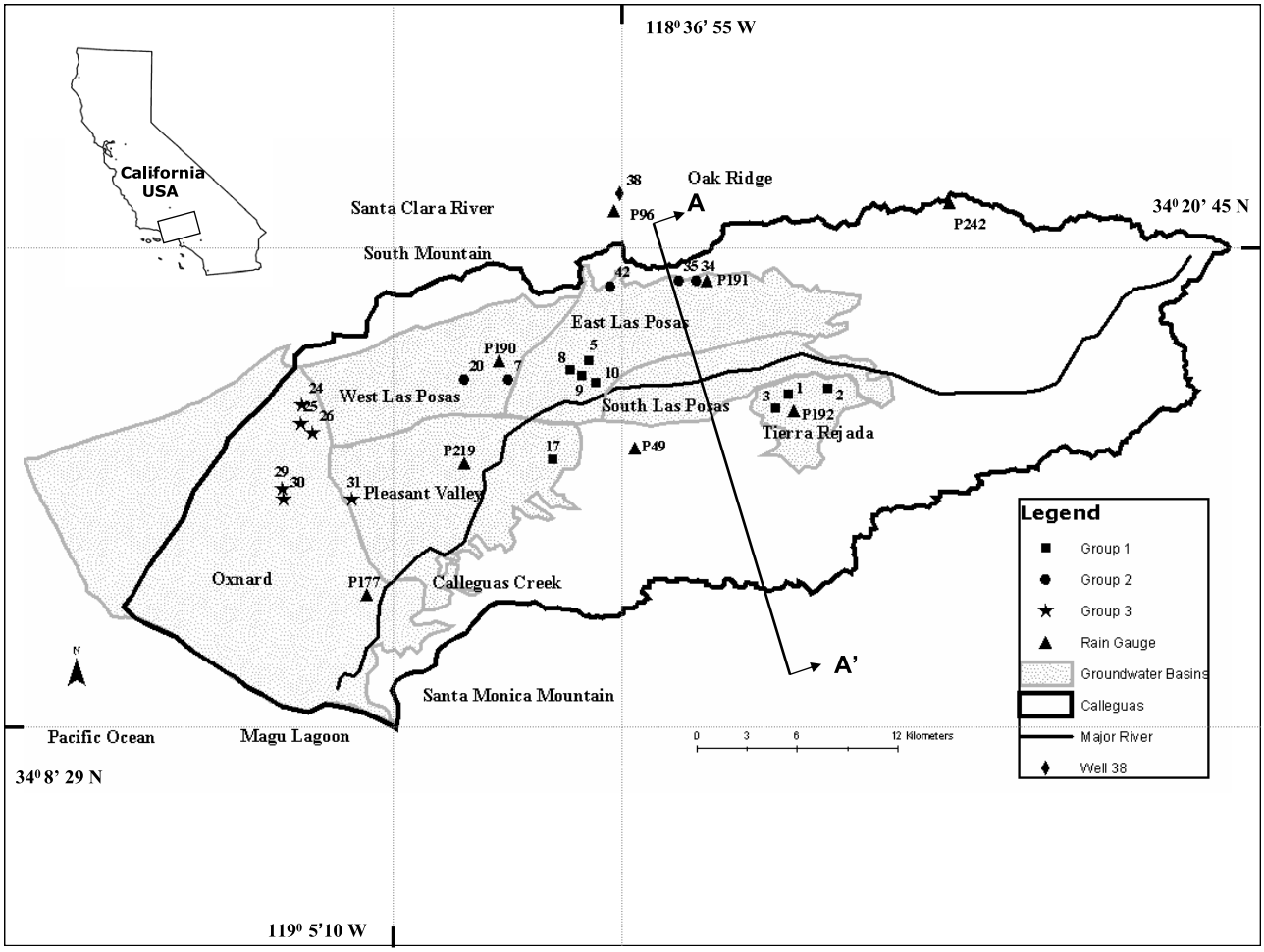

Figure 1. Map of Calleguas Creek watershed, including groundwater subbasins, rain gauge locations, and selected groundwater wells, with the trace of cross section A-A′ (shown in Figure 2).

the Santa Susana and Santa Monica Mountains with elevations in excess of 1000 m. Topography in this area is typified by rugged, mountainous terrain. Moving in a southwesterly direction toward sea level, the watershed consists of rolling hills, alluvial valleys, coastal floodplains and, ultimately, Mugu Lagoon.

[9] Historically, Calleguas Creek and its tributaries (Revolon Slough, Conejo Creek, Arroyo Santa Rosa, Arroyo Conejo, Arroyo Las Posas, and Arroyo Simi) were intermittent and flowed seasonally from the headwaters near the City of Simi Valley onto the Oxnard Plain [*California Regional Water Quality Control Board*, 1994]. Due to urbanization, Calleguas Creek is now primarily a perennial stream fed by treated wastewater flows, with secondary surface flows originating from increasing groundwater levels, agricultural and urban runoff, and periodic storm water flow [*CCWMP*, 2004].

[10] Groundwater is primarily contained within the Fox Canyon aquifer system (Figure 2), which is linked to the neighboring (north) Santa Clara River watershed. Groundwater basins include the Las Posas Valley, Pleasant Valley, Simi Valley, Santa Rosa, Tierra Rejada, and the Oxnard Plain, which is a subbasin of Santa Clara groundwater basin. The Calleguas–Santa Clara groundwater aquifer system experiences seawater intrusion, interaquifer flow, land subsidence, groundwater contamination and streamflow depletion as a consequence of the increasing population and steady development of water resources in the region [*Hanson et al.*, 2003]. Urban water needs are met principally through imported water. Agricultural water demands have historically been satisfied from the Fox Canyon groundwater aquifer system and imports of surface water from the neighboring Santa Clara River Watershed.

[11] The current study includes analysis of wells located in Las Posas Valley, Pleasant Valley, Tierra Rejada and Oxnard basins (Table 1). The Las Posas Valley groundwater basin encompasses a surface area of 171 km^2 and is bounded on the north by South Mountain and Oak Ridge, on the south by the Camarillo and Las Posas Hills, on the east by the Santa Susana Mountains and on the west by the Oxnard subbasin of the Santa Clara River Valley Groundwater Basin [*CDWR*, 2003]. The basin has been subdivided into West Las Posas, East Las Posas, and South Las Posas (Figure 1). The South Las Posas Basin is separated from the East Las Posas Basin by an east-west slope in the subsurface. The East Las Posas Basin is separated from West Las Posas by a north trending fault, across which groundwater levels differ by as much as 122 m. The West Las Posas Basin is isolated from the South and East Las Posas basins by a north-south fault, and is hydrologically connected to the Oxnard Plain Basin [*Fox Canyon Groundwater Management Agency*, 2006].

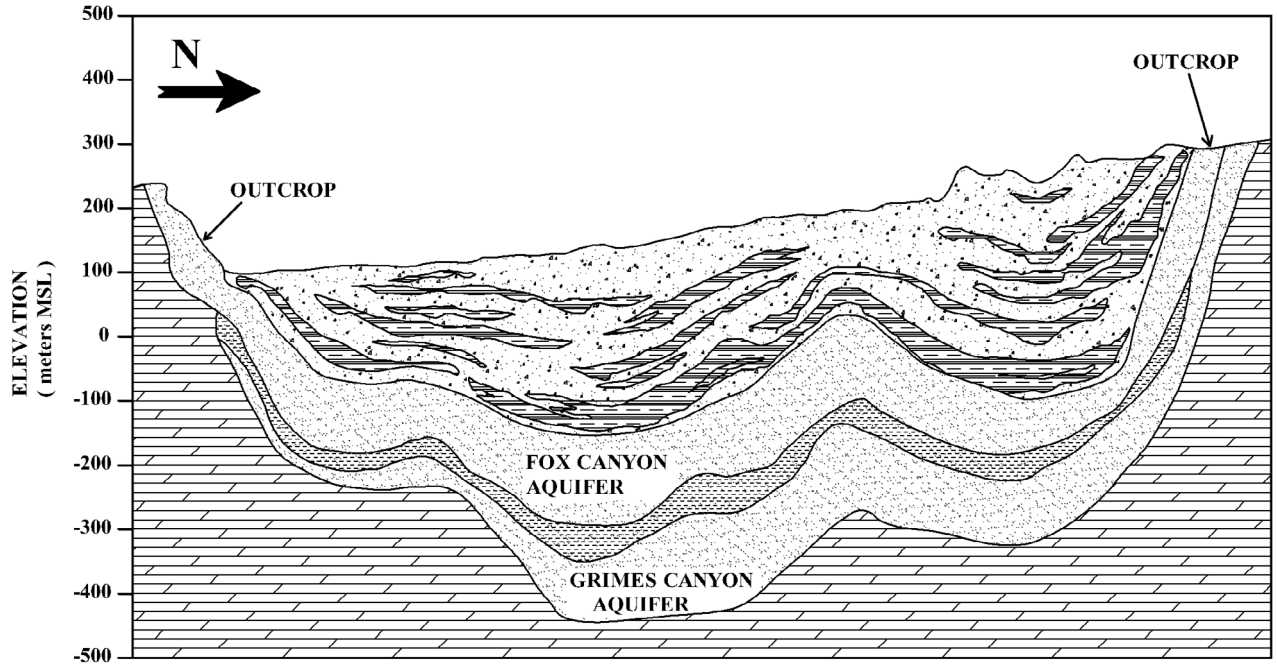

Figure 2. Cross-sectional profile (A′-A) from Figure 1.

Groundwater recharge to the basins comes predominantly from percolation of precipitation across outcrops of the Fox Canyon and Grimes Canyon gravels as well as channel recharge. Injection of imported water and irrigation and septic system return occurs in the eastern portion of the basin [*CCWMP*, 2004].

[12] The Pleasant Valley basin has a surface area of 87 km^2. The basin is bounded on the north by the Camarillo and Las Posas Hills, on the south by the Santa Monica Mountains, on the east by Arroyo Santa Rosa, and on the west by the Oxnard subbasin [*CDWR*, 2003]. Groundwater recharge to the basin comes primarily from subsurface flow across the Springville fault zone, through Fox Canyon gravels from the Arroyo Santa Rosa Valley Basin, and through fractures in the volcanic rocks. Irrigation water and septic system effluent also contribute to basin recharge.

[13] The Tierra Rejada basin has a surface area of 17.9 km^2. The basin is bounded on the south and east by surface drainage divides and on the north and west by faults that restrict groundwater flow. An unnamed north trending fault forms the western boundary and the east trending Simi fault is the northern boundary [*CDWR*, 2003]. Tierra Rejada groundwater recharge is provided through percolation of rainfall, streamflow, and irrigation return. Minor amounts of water are added to the aquifer from septic systems and a wastewater treatment plant.

[14] Finally, the Oxnard basin is a subbasin of the Santa Clara River Valley basin. The northern boundary coinciding with a portion of the Oak Ridge fault, the southern boundary is formed by contact of permeable alluvium with the semipermeable rocks of the Santa Monica Mountains. The eastern edge of the subbasin lies against the Pleasant Valley and Las

Table 1. Groundwater Basin Characteristics Within the Calleguas Creek Watershed[a]

Groundwater Basin	Water-Bearing Formation	Principal Aquifer	Condition of Groundwater Occurrence	Storage Capacity (m^3)
Las Posas Valley[b]	Recent and Upper Pleistocene alluvium[c]	Lenses of permeable sediments	Unconfined	1.54E+09
Lower aquifer zone	San Pedro Formation[d]	Fox Canyon and Epworth Gravels aquifers	Confined, except near outcrop	
Lower aquifer zone	Santa Barbara Formation[e]	Grimes Canyon aquifer	Confined, except near outcrop	
Pleasant Valley	Recent and Pleistocene alluvium	Permeable lenses not connected with Oxnard aquifer	Confined and unconfined	2.33E+09
Oxnard Plain Forebay Area	Recent and Pleistocene alluvium	Oxnard, Mugu, Hueneme, and Fox Canyon aquifers	Unconfined and confined	1.57E+09
Oxnard Plain Pressure Area	Recent alluvium	Semiperched water-bearing zone, and Oxnard aquifer	Unconfined in Semiperched, Confined in Oxnard	1.11E+10
Tierra Rejada	Volcanics	Fracture zones	Essentially unconfined	4.85E+07

[a]Information from the Ventura County Watershed Protection District and *CDWR* [2003].
[b]West and East Las Posas.
[c]Pleistocene alluvium consists of silts and clays with lenses of more permeable sand and gravel.
[d]San Pedro Formation consists dominantly of fine material with scattered lenses of sands and gravels.
[e]Santa Barbara Formation consists of fine gravel deposits.

Table 2. Precipitation Gauges Used in This Study

Gauge	Name	Elevation (m)
P49	Santa Rosa Valley-Worthington Ranch	137
P177	Camarillo-Pacific Sod	6
P190[a]	Somis-Bard	140
P191	Moorpark-Downing Ranch	317
P192	Moorpark-Everett	207
P219	Camarillo-Hauser	52
P96[b]	Bardsdale-Young Ranch	400

[a]The precipitation gauge selected for the analysis.
[b]Used for PDO analysis.

Posas Valley basins. Recharge in the Oxnard basin comes from percolation of surface flow from the Santa Clara River. Subsurface flow from Santa Paula subbasin makes its way over or across the Oak Ridge fault, and some underflow may come from the Las Posas and Pleasant Valley Basins on the east. Irrigation and septic system return also occurs in the basin. The coastal portion of the aquifer is subject to heavy seawater intrusion and land subsidence [*Hanson et al.*, 2003]. More details on the physical characteristics of the basins are reported by *CDWR* [2003] and *Hanson et al.* [2003].

2.2. Calleguas Creek Hydroclimatology

[15] The Calleguas Creek watershed experiences the typical Mediterranean climate found in the southern California coastal region. Summers are relatively warm and dry, while winters are mild and wet. Annual rainfall averages 380 mm in the lower plains (Camarillo Houser, gauge P219) (Figure 1) and up to 580 mm in the upper portions of the Calleguas watershed (Tripas Canyon, gauge P242) (Figure 1). Calleguas Creek watershed receives the majority of its precipitation (approximately 85%) during the winter season, which extends from November through March. The wettest year during the 1975 to 2004 study period was 1983, corresponding to the strongest El Niño episode in our record, with a total precipitation of 790 mm in the lower plains (P219) (Figure 1) and 1240 mm in the upper portions (P242) (Figure 1). The lowest annual rainfall (135 mm at P219 and 212 mm at P242) was observed in 1989, which corresponds with the strongest La Niña episode in our record (1988–1989 event). Temperatures typically range from 10°C (low) to 25°C (high) in Simi Valley (upper watershed), and 12°C to 18°C at Magu Lagoon (outlet). Potential evapotranspiration (PET) in the watershed ranges from about 760 mm/yr near the coast to 960 mm/yr in the upper watershed (California Irrigation Management Information System, http://wwwcimis.water.ca.gov/cimis/data.jsp).

2.3. Hydrologic and Climatologic Data

[16] Hydrologic time series have been collected for the period 1975–2004 within the study area. The analysis period was chosen based on the length and completeness of data records. Seven rain gauges from the Ventura County Watershed Protection District (VCWPD) were selected to represent precipitation over the study basins (Table 2 and Figure 1). Data from 311 groundwater pumping wells were obtained from Calleguas Municipal Water District. A subset of wells (20) was selected for further study based on overlapping time periods, completeness of record, and the correlation between wells. The selected wells are spatially distributed as follows: seven wells within East of Las Posas basin, two wells located in West Las Posas basin, two wells in Pleasant Valley basin, three wells in Tierra Rejada basin, five wells within Oxnard basin and one well in the Fillmore basin (Figure 1 and Table 3). Data from a single well (with longer records), located in Filmore basin (W38) (Table 3), were used to explore the linkages between groundwater fluctuations and the Pacific Decadal Oscillation (PDO). This well was from the Fillmore basin, part of the Santa Clara Valley basin just to the north of the Calleguas watershed (Figure 1). A period of 30 years was assembled for the 19 primary wells and a period of 50 years was gathered for the Fillmore basin well. In addition, time series of water extraction (1983–2004) from two wells (W7 and W8) (Table 3) were used to assess the influence of

Table 3. General Characteristics for Study Wells, Including Primary Use, Surface Elevation, Depth, Bottom Elevation, and Location[a]

Well Number	Group	Depth Code	Use	Elevation (m)	Depth (m)	Elevation at Well Bottom (m)	Basin Name
W1	1	None	Unused	191	106	84	Tierra Rejada
W2	1	None	Irrigation	212	151	61	Tierra Rejada
W3	1	None	Unused	184	137	47	Tierra Rejada
W5	1	Lower	Irrigation	151	-	151	East Las Posas
W8	**1**	**Lower**	**Domestic-Irrigation**	**129**	**335**	**−206**	**East Las Posas**
W9	1	Both	Irrigation	134	271	−137	East Las Posas
W10	1	Both	Unused	122	173	−50	East Las Posas
W17	1	Both	Unused	44	247	−202	Pleasant Valley
W7	**2**	**Lower**	**Irrigation**	**124**	**440**	**−316**	**West Las Posas**
W20	2	Lower	Irrigation	128	564	−436	West Las Posas
W34	2	Lower	Irrigation	325	335	−11	East Las Posas
W35	2	Lower	Industrial	323	335	−13	East Las Posas
W42	2	Lower	Industrial	330	462	−132	East Las Posas
W24	**3**	**Lower**	**Irrigation**	**35**	**453**	**−418**	**Oxnard**
W25	3	Lower	Irrigation	32	333	−302	Oxnard
W26	3	Lower	Domestic	35	290	−255	Oxnard
W29	3	Upper	Unused	18	46	−28	Oxnard
W30	3	Lower	Irrigation	18	306	−289	Oxnard
W31	3	Lower	Irrigation	21	358	−337	Pleasant Valley
W38[b]		Upper	Domestic	116	28	88	Fillmore

[a]Key wells are indicated with bold.
[b]For PDO analysis.

pumping on the groundwater level variations, as well as possible linkages with climate variation. The water extraction data were available in six month increments (i.e., total withdrawal from January–June and July–December).

[17] Precipitation data were available on a daily basis and water level observations were primarily available every two months. Daily precipitation amounts were aggregated to monthly values and well water levels were linearly interpolated to obtain monthly values. Data at the monthly or yearly scale can generally be used for examination of climatic modes [*Fleming et al.*, 2002]; hence, a monthly temporal resolution was chosen given our study goals and the available data. To ensure a uniform (temporal) comparison between the data types, a 3 month running mean was calculated for both precipitation and water level data during the study period. Water level variability was analyzed for the 19 individual wells and a correlation matrix was computed to establish well locations (or groups) with similar hydrologic behavior. Both precipitation and well data time series were detrended, using a low-order polynomial. Detrending removes a portion of the larger quasiperiodic cycles and also partially eliminates anthropogenic (urbanization) signals from groundwater levels [*Hanson et al.*, 2004]. The series were also detrended to maintain consistency among the various data types analyzed. Detrended series were standardized by the mean and standard deviation to facilitate comparisons between data types.

[18] The Oceanic El Niño Index (ONI) was used to represent the ENSO signal. The ONI is defined as the 3 month running mean sea surface temperature (SST) departures in the Niño 3.4 region [*Smith et al.*, 2008]. A positive ONI greater than or equal to +0.5°C indicates El Niño (warm phase) and a negative ONI less than or equal to −0.5°C indicates La Niña (cool phase). A time series of the 3 month running mean of ONI was obtained from the Climate Prediction Center (http://www.cpc.noaa.gov/). Monthly series of PDO were obtained from the University of Washington (http://jisao.washington.edu/pdo/PDO.latest). The PDO Index is defined as the leading principal component of North Pacific monthly sea surface temperature variability.

2.4. Correlation Analysis

[19] A spatial correlation matrix was estimated to determine well locations or groups with similar hydrologic behavior and to facilitate selection of key wells for further analyses. Identification of highly correlated water level data is also beneficial for water management purposes, as data from correlated wells can provide information for those periods when data from other (correlated) monitoring wells is not available.

[20] The time series observed at well W_j and characterized by n_j values is indicated here as $x_{j,k}$, $k = 1,\ldots,n_j$. In order to evaluate the correlation between two wells (W_i, W_j), the ijth element of the covariance matrix is estimated as

$$Cov_{ij} = E\left[(x_i - \mu_i)(x_j - \mu_j)\right] = \frac{1}{N}\sum_{k=1}^{N}(x_{i,k}-\mu_i)(x_{j,k} - \mu_j) \quad (1)$$

where E is the mathematical expectation and $\mu_i = \frac{1}{N}\sum_{k=1}^{N} x_{i,k}$. The correlation matrix is defined as the $[N_{well} \times N_{well}]$ matrix that contains the spatial correlation coefficient between two wells (W_i, W_j). The spatial correlation coefficient, ρ_{ij}, is defined as

$$\rho_{ij} = \frac{Cov(x_i, x_j)}{\sqrt{Cov(x_i, x_i)} \cdot \sqrt{Cov(x_j, x_j)}} \quad (2)$$

The correlation coefficient indicates the strength of the temporal relationship between every two wells. Values equal to zero indicates that the two wells are not temporally correlated, while a value close to 1 indicates high correlation.

2.5. Time Series Autocorrelation

[21] Prewhitening was suggested by *von Storch* [1995] to reduce the influence of serial correlation on the Mann-Kendall test. The serial correlation component, such as a lag-one autoregressive process AR(1) is removed from the time series prior to applying the Mann-Kendall test. This method has been used in trend detection studies [*Khaliq et al.*, 2008; *Koutsoyiannis and Montanari*, 2007, *Yue et al.*, 2003; *Douglas et al.*, 2000]. Time series can be prewhitened using the following equation:

$$Y_t = X_t - r_1 X_{t-1} \quad (3)$$

where Y_t is the prewhitened time series, X_t is the raw time series and r_1 is the lag-one serial correlation coefficient.

2.6. Trend Estimation

[22] The Mann–Kendall is a nonparametric statistical test based on the correlation between the ranks of a time series and their time order [*Kendall and Gibbons*, 1990]. The test statistic S_j is calculated assuming the null hypothesis that the series $x_{j,k}$, $k = 1,\ldots,n_j$ is a realization of n_j independent and identically distributed random variables. A positive value of S_j indicates upward trends whereas a negative S_j value indicates downward trends. The Mann-Kendall statistic (S) is given by

$$S_j = \sum_{k=1}^{n_j-1}\sum_{i=k+1}^{n_j} sgn\left(x_{j,i} - x_{j,k}\right) \quad (4)$$

where sgn(x) is equal to −1, 0, +1 if $(x_{j,i} - x_{j,k})$ is negative, zero or positive, respectively. The statistic S_j is characterized by a normal distribution with zero mean and a variance $Var\,[S_j]$ given by

$$Var\left[S_j\right] = \frac{1}{18}\left\{n_j(n_j-1)(2n_j+5) - \sum_{p=1}^{q} t_{p_j}(t_{p_j}-1)(2t_{p_j}+5)\right\} \quad (5)$$

where q is the number of tied groups (a tied group is a set of sample data having the same value), t_p denotes the number of data points in the pth group, and Σt_p indicates the summation over all ties. When $n_j > 0$ the standard normal variate Z is calculated as

$$Z_j = \begin{cases} \dfrac{S_j - 1}{\sqrt{Var\,(S_j)}} & if \quad S_j > 0 \\ 0 & if \quad S_j = 0 \\ \dfrac{S_j + 1}{\sqrt{Var\,(S_j)}} & if \quad S_j < 0 \end{cases} \quad (6)$$

Table 4. Identification of Well Groups and Key Wells Determined by Correlation Analysis[a]

Group Number	Well Number	Average Correlation Coefficient	Key Well
1	W1, W2, W3, W5, W8, W9, W10, W17	0.90	W8
2	W7, W20, W34, W35, W42	0.83	W7
3	W24, W25, W26, W29, W30, W31	0.80	W24

[a]The threshold for inclusion within a group is a correlation (R^2) > 0.70.

The null hypothesis is accepted if $|Z_j| \leq Z_{j,\alpha/2}$ in a two-sided test of significance, where α indicates the significance level. Otherwise, the null hypothesis is rejected and the existence of a monotonic trend (not necessarily linear) is concluded. In this study, if $|Z_j| \leq Z_{j,\alpha/2}$ the trend is not significant.

2.7. Spectrum Estimation

[23] Frequency analysis for all study time series was performed utilizing fast Fourier transform [*Welch*, 1967], which transforms the data from the time domain into the wave number/frequency domain [*Kao*, 1968]. This technique effectively decomposes the signal into a linear superposition of sinusoids of different frequencies. The general expression for the Fourier transform, derived from *Newland* [1993], is

$$X_j(\omega) = \sum_{k=1}^{N} x_j(k) e^{-i\omega k} \tag{7}$$

where i is the imaginary unit and ω is the frequency of the kth wave or mode. Since $X(\omega)$ is a complex valued functions, we can take its square modulus, which represents the power associated with the kth wave number. The power indicates the relative importance of that basis function with respect to all the others, and is also representative of the relative energy (or variance) associated with that particular wave.

[24] A number of more or less sophisticated tools are available to infer the periodicity in time series, e.g., autoregressive models, maximum entropy spectral analysis, singular spectrum analysis, wavelet analysis [*Box and Jenkins*, 1976; *Salas et al.*, 1988; *Padmanabhan and Rao*, 1988; *Smith et al.*, 1998; *Hanson et al.*, 2004; *Gurdak et al.*, 2007; *Torrence and Compo*, 1998; *Echer et al.*, 2008]. Nevertheless, contrasting with other statistical methods, the Fourier approach does not require educated (preconceived) guesses as to the frequency content of the signal, allowing effective empirical determination of the full spectrum [*Fleming et al.*, 2002].

[25] Prior to applying Fourier analysis the time series were detrended using a low-order polynomial. Residuals for the time series were obtained by subtracting the detrending polynomial from the raw time series.

3. Results and Discussion

3.1. One Correlation Matrix and Key Wells

[26] A subset of 19 wells was selected for further study based on a homogenous time period and a threshold correlation of $R^2 > 0.70$ between wells. Based on analysis of the 19 primary wells, three groups with similar hydrological behavior (water level response) were identified: group 1 (8 wells); group 2 (5 wells); and group 3 (6 wells). The group characteristics are summarized in Tables 3 and 4 and the spatial location of all the wells is shown in Figure 1. Group 1 is the most homogenous and exhibits the highest average correlation (0.90) between wells, group 2 has an average correlation of 0.83, and group 3 displays an average correlation of 0.80. Group 1 is composed primarily of wells located in Tierra Rejada and East Las Posas basins and one well (W17), located in the Pleasant Valley basin, which shows the lowest average correlation (0.82) within the group. Four wells from this group are not currently utilized for water supply and the remaining four wells are used primarily for irrigation purposes. Group 2 is composed of three wells located in East Las Posas and two wells located in West Las Posas, with well W35 showing lowest average correlation (0.79). Three wells of this group are used for irrigation purposes and two for industrial supply. Five wells in group 3 are located in the Oxnard basin, while the sixth well is located in the Pleasant Valley basin. The lowest correlation is seen in well W29 (average correlation of W29 with wells of the same group is 0.77), located in the Oxnard basin. Wells in this group are mainly used for irrigation purposes. To highlight results from each of the three groups, a representative (key) well was selected based on the value of the correlation coefficient. Well W8 (domestic and irrigation purposes, East Las Posas basin) was selected as the key well for group 1. The key well for group 2 is well W7 (irrigation, West Las Posas basin) and the key well for group 3 is W24 (irrigation, Oxnard basin). These key wells are used for the following annual cycle analysis.

3.2. Mean Annual Cycles

[27] Mean monthly rainfall values recorded at the gauges distributed over the five groundwater basins are highlighted in Figure 3a. The similarities of the waveforms are very close for all the time series. Peak rainfall is observed in February, while the lowest precipitation is observed in July. As expected, the highest precipitation values are observed in rain gauges located in the upper elevations of the watershed while lower values of precipitation occur in the lower elevations. The mean monthly values for water levels in the select key wells are also presented (Figure 3b). In general, the peak of the mean monthly values of the well levels is lagged approximately 1.5 months with respect to the precipitation peak, highlighting the temporal lag in the aquifer response from natural recharge. Observed differences in the groundwater levels and precipitation maximum values may also be associated with anthropogenic influences. For example, higher groundwater levels can be linked with reduced groundwater withdrawals during the wetter months and vice versa. Slight differences in the mean monthly values for the highlighted wells can be related to variations in soil heterogeneity, screen depths and withdrawal pumping rates at each of the sites. Tukey's "schematic" box plots [*Chambers et al.*, 1983] were used to describe the variability in monthly precipitation and well level data (Figure 4). Higher variance is observed for precipitation; indicating stronger intra-annual variability in the rainfall time series. In general, precipitation data are also more skewed, while the well water level data are more symmetric about the mean. Infiltration processes, travel time and other factors significantly dampen the precipitation signal

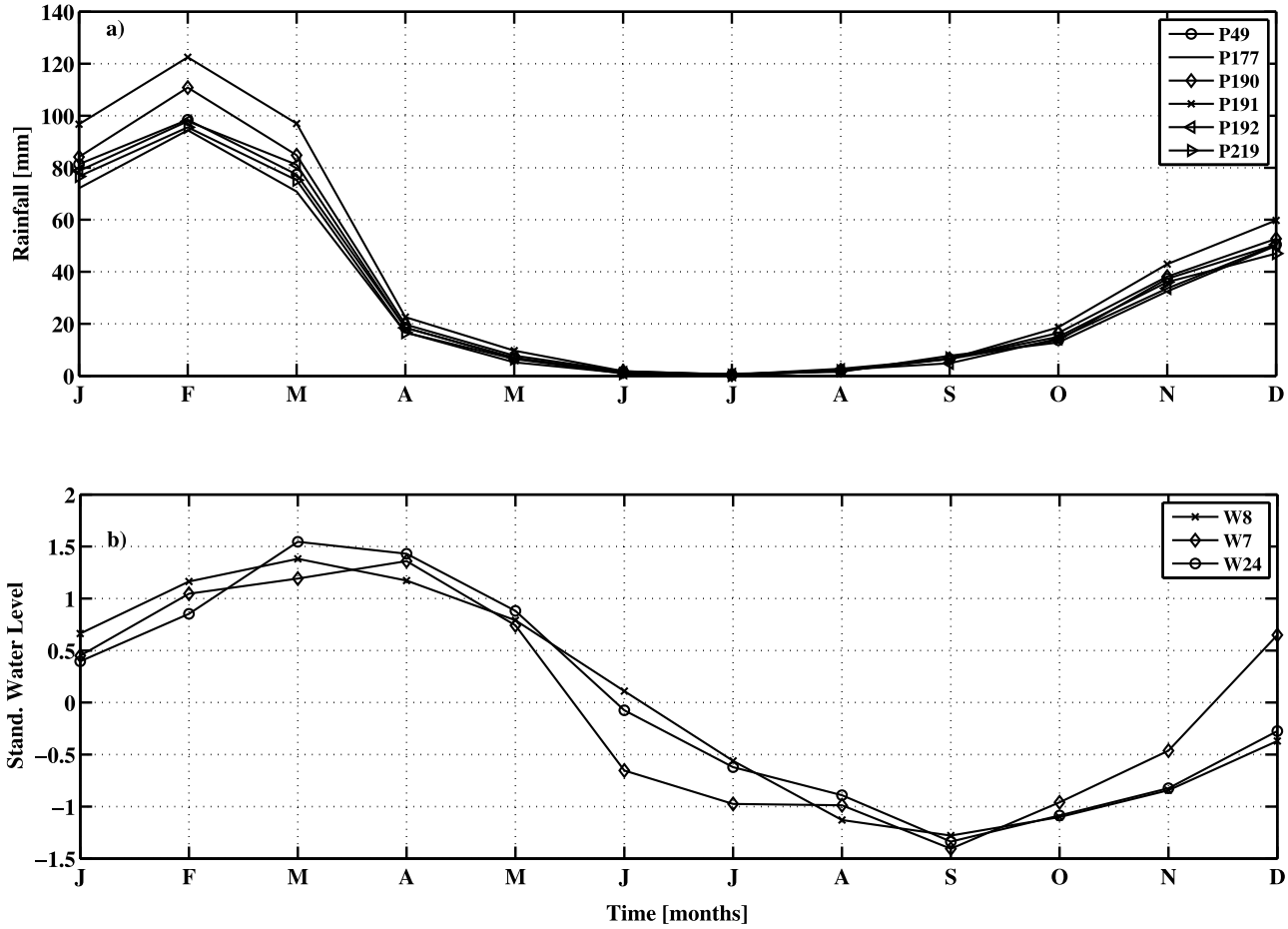

Figure 3. (a) Mean annual cycle of precipitation (averaged from 1975 to 2004) for each of the precipitation gauges over the study area and (b) standardized mean annual cycle of water levels for the selected key wells (W8, group 1; W7, group 2; and W24, group 3).

as it travels through the subsurface, resulting in a smoother and more consistent groundwater response.

3.3. Trend Analysis

[28] The Mann-Kendall test was used to detect and assess significance levels of possible trends in the monthly time series of precipitation and groundwater levels for all study wells. Prior to applying the Mann-Kendall test a prewhitened analysis was performed in the raw series as described in section 2.5. The results of this analysis are summarized in Table 5. The precipitation time series does not show a statistically significant trend (decided on a probability level of

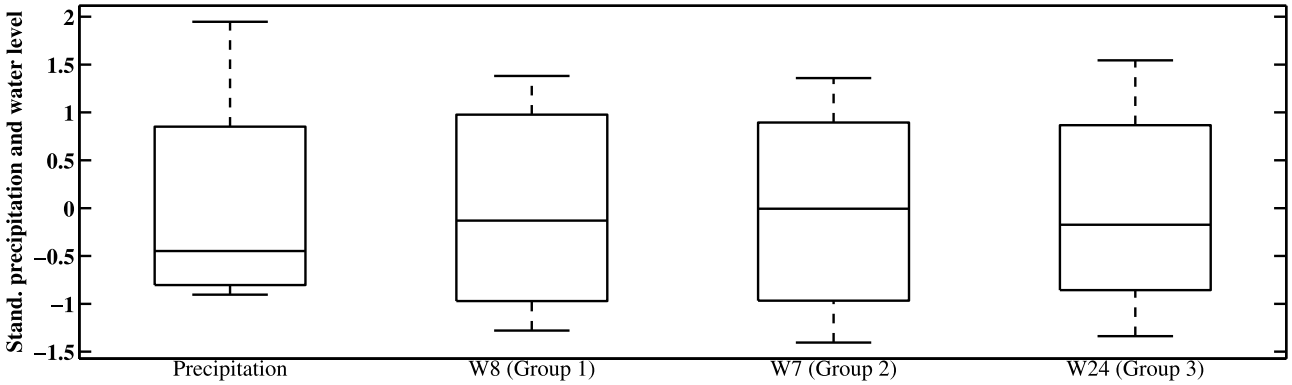

Figure 4. Box plots representing the distribution of standardized average annual cycle of precipitation and water levels for wells W8 (group 1), W7 (group 2), and W24 (group 3). Top and bottom edge of each box represents the 75th and 25th percentiles, respectively; whiskers extend from each end of the box to the last data point within 1.5 times the interquartile range; and the line bisecting the box represents the median.

Table 5. Mann-Kendall Results for the Water Level Time Series of Studied Wells[a]

Well Number	Group	Original p Value	$\text{Trend}_{\text{original}}$	$\alpha_{\text{original}} = 0.05$[b]	$\text{Trend}_{\text{whitened}}$	$\alpha_{\text{whitened}} = 0.05$[b]	Percent Persistence Explained
W1	1	0.000	(+)	yes	(−)	Yes	99
W2	1	0.000	(+)	yes	(−)	yes	99
W3	1	0.000	(+)	yes	(−)	yes	99
W5	1	0.000	(+)	yes	(+)	no	99
W8	**1**	**0.000**	**(+)**	**yes**	**(+)**	**no**	**99**
W9	1	0.000	(+)	yes	(+)	no	99
W10	1	0.000	(+)	yes	(−)	no	99
W17	1	0.000	(+)	yes	(−)	yes	99
W7	**2**	**0.000**	**(−)**	**yes**	**(−)**	**no**	**98**
W20	2	0.000	(−)	yes	(−)	no	98
W34	2	0.000	(−)	yes	(−)	yes	95
W35	2	0.000	(−)	yes	(−)	yes	94
W42	2	0.000	(−)	yes	(−)	yes	94
W24	**3**	**0.000**	**(+)**	**yes**	**(+)**	**no**	**93**
W25	3	0.002	(−)	yes	(−)	no	95
W26	**3**	**0.459**	**(−)**	**no**	(−)	no	90
W29	3	0.000	(+)	yes	(+)	no	97
W30	**3**	**0.098**	**(−)**	**no**	(−)	no	92
W31	3	0.000	(+)	yes	(+)	no	92
W38[c]		**0.054**	**(−)**	**no**	(−)	no	95

[a]Shown are trend analysis results for original series and whitened series. Key wells are indicated with bold.
[b]Significance at $\alpha = 0.05$.
[c]For PDO analysis.

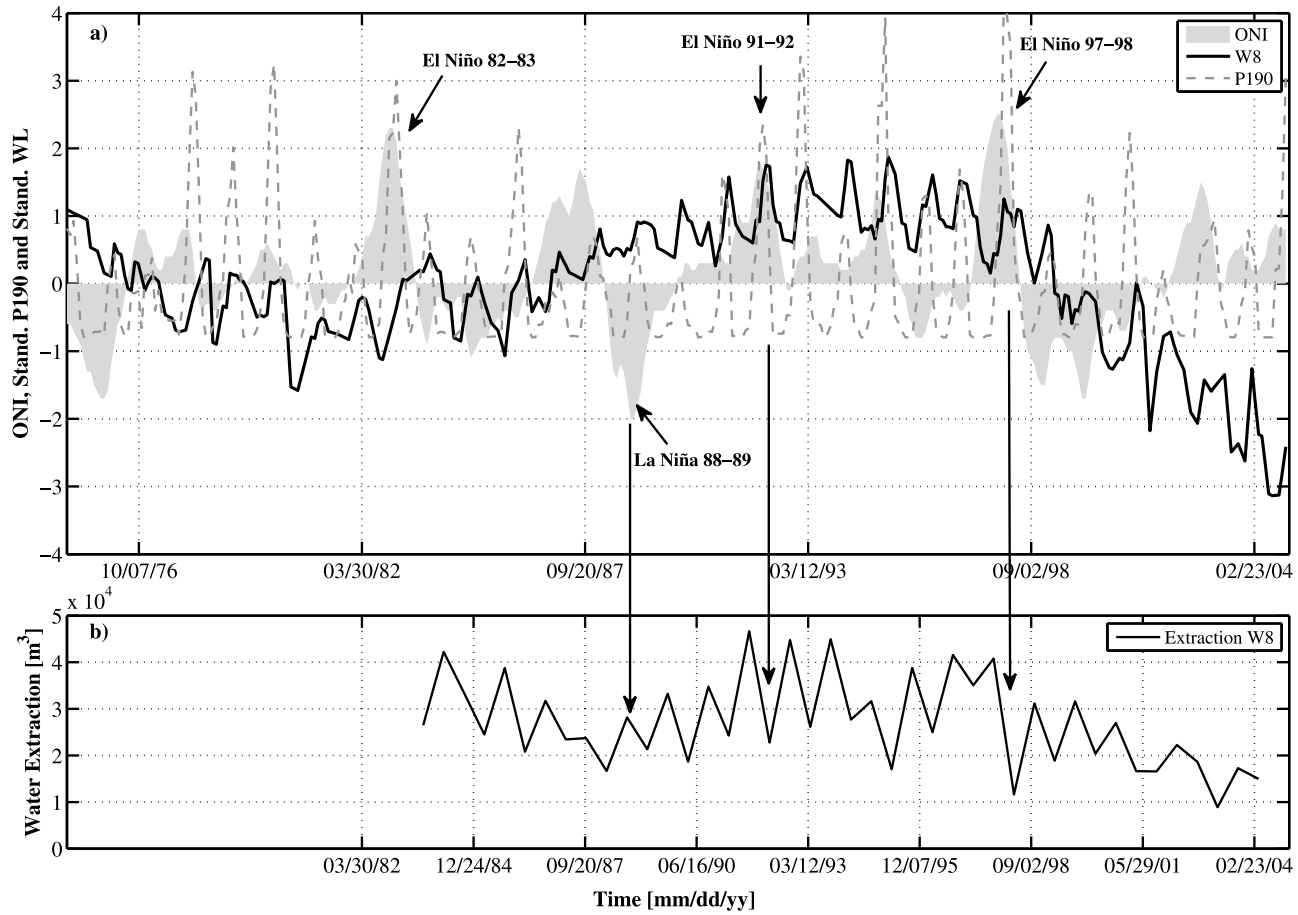

Figure 5. Time series analysis for (a) detrended standardized 3 month running mean for precipitation (P190), water levels in well W8 (group 1), and the El Niño–Southern Oscillation index (ONI) and (b) water extraction data for well W8. Pumpage values are plotted at the midpoint of the 6 month period.

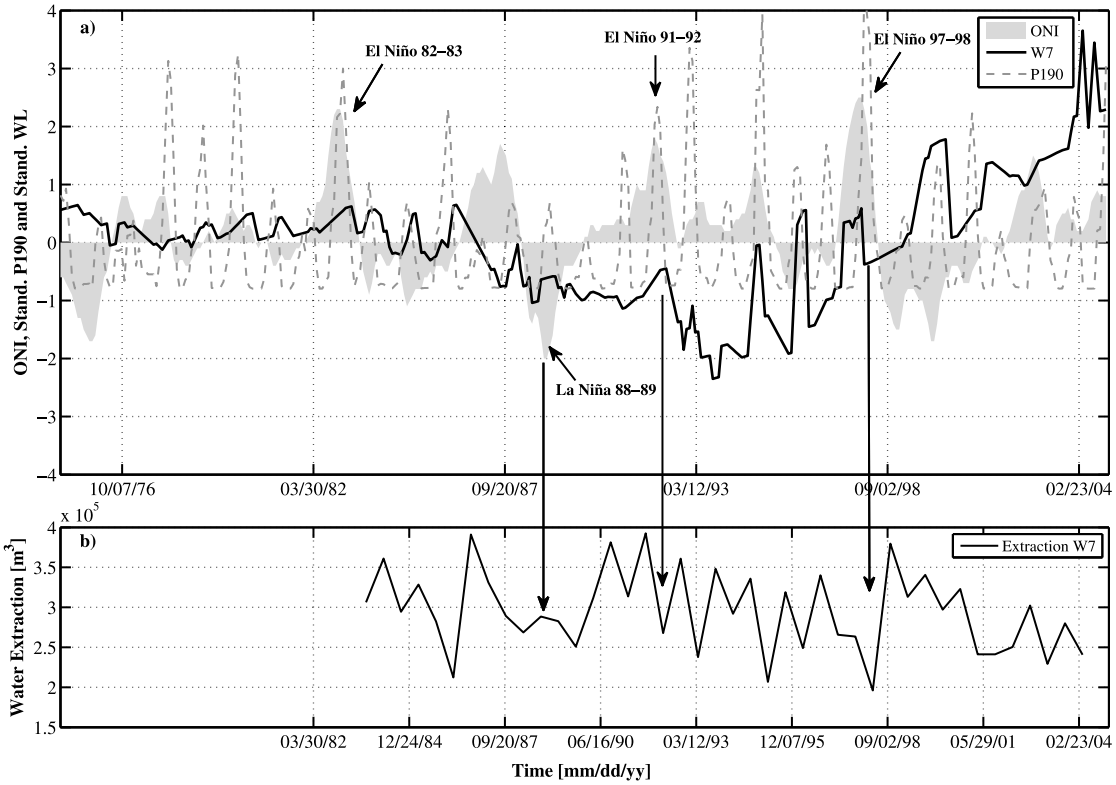

Figure 6. Same as Figure 5 except for W7 (group 2).

significance of 95%), with all calculated trends observed as slightly negative but nonsignificant (all p values are > 0.05). We note that these results are valid for our period of analysis (1975–2004) and that nonpersistent trends could be present previous to this period. In contrast, the water level time series show noticeable trends. The prewhitening analysis identified high persistence (serial correlations) in the groundwater time series levels. Persistence among the wells ranges from 66% to 99%. The autocorrelation faction (ACF) reveals that in most of the cases none of the autocorrelations of the AR(1) model residual are outside the 99% confidence interval around zero. Whiteness of residuals was also checked with the Portmanteau test. Review of the individual correlations of residual and Portmanteau tests confirmed the AR(1) model as an effective model for evaluating persistence in the groundwater level series. The Mann-Kendall test, applied to the original series, identifies a significant upward trend in wells in group 1, while group 2 shows a significant downward trend (Table 5). Group 3 includes three wells with a positive (increasing) trend and three wells that exhibits a negative trend (trends in two of the wells are nonsignificant). The Mann-Kendall test was also applied to the whitened time series. This analysis identifies a significant downward trend in wells W1, W2, W3, W10 and W17, while a nonsignificant upward trend was observed in wells W5, W8 and W9 from group 1. Group 2 shows a significant downward trend for well W34, W35 and W42, while a nonsignificant downward trend was seen for wells W7 and W20. Group 3 includes three wells with a nonsignificant positive (increasing) trend and three wells that exhibit a nonsignificant negative trend.

[29] The response in the groundwater levels can be directly related to precipitation fluctuation and, theoretically, to regional El Niño signals. The detrended and standardized three month running mean time series for rain gauge P190 along with the El Niño–Southern Oscillation (ONI) index are plotted together with the (detrended and standardized) water level time series of the three key wells (Figure 5, group 1 (W8); Figure 6, group 2 (W7); Figure 7, group 3 (W24)). Water extraction for W8 and W7 are also shown in Figures 5 and 6, respectively (extraction data are not available for well W24). This data consist of groundwater volumes extracted over 6 month period. In general, during El Niño events, southwestern U.S. cold season precipitation tends to be higher than normal, and during La Nina events, precipitation is typically less than normal [*Hidalgo and Dracup*, 2003]. An overall positive anomaly in precipitation is also observed related with El Niño (ENSO warm phase) (Figure 5). A strong rainfall response is observed during two strong El Niño events (1982–1983, 1991–1992 and 1997–1998), but there is also a strong precipitation response for two weak to moderate El Niño events (1977–1978 and 1994–1995). A strong rainfall response is also noted during 1979–1980 for a period that is not recorded as an El Niño event. The La Niña (ENSO cold phase)–precipitation relationship is less pronounced with weak to moderate La Niña phases showing either negative or positive signals in precipitation. The strongest La Niña event was observed in 1988–1989 and the precipitation peak is observed as above normal (also noted by *Hanson and Dettinger* [2005]). Linkages between precipitation and ENSO signals have been observed in other studies in southern California [*Schonher and Nicholson*, 1989; *Mo and Higgins*, 1998; *Cayan et al.*, 1998; *Cook and Schaefer*, 2008]. Pumping values are general higher during the second

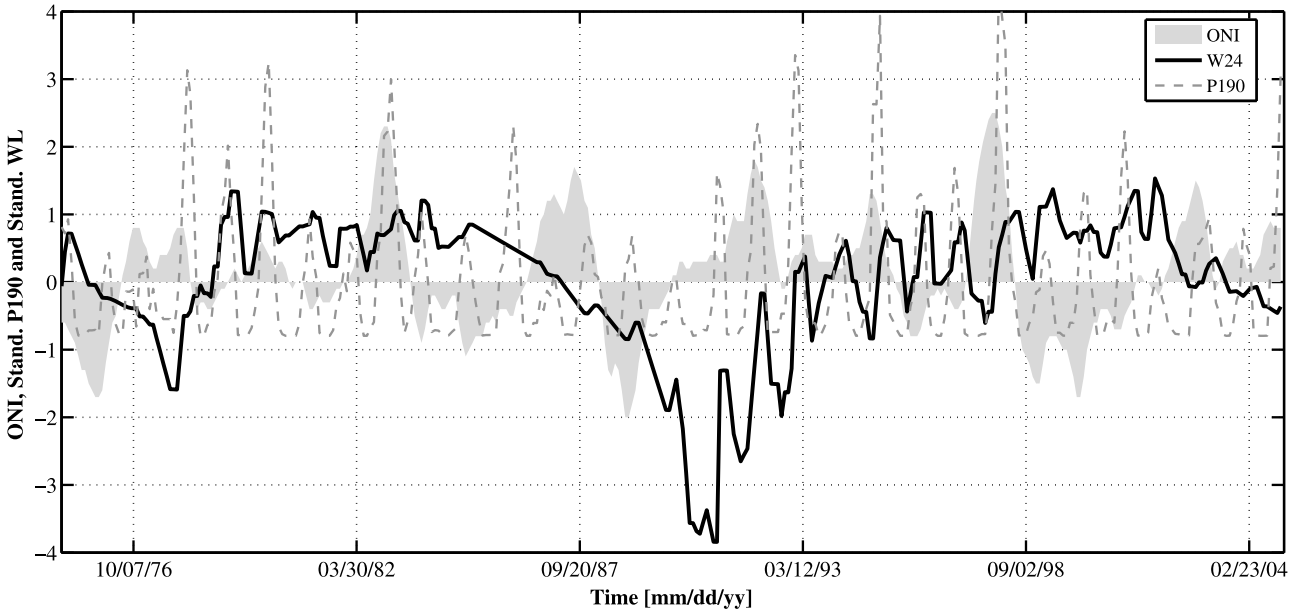

Figure 7. Same as Figure 5a except for W24 (group 3). Pumpage data for W24 (group 3) were not available.

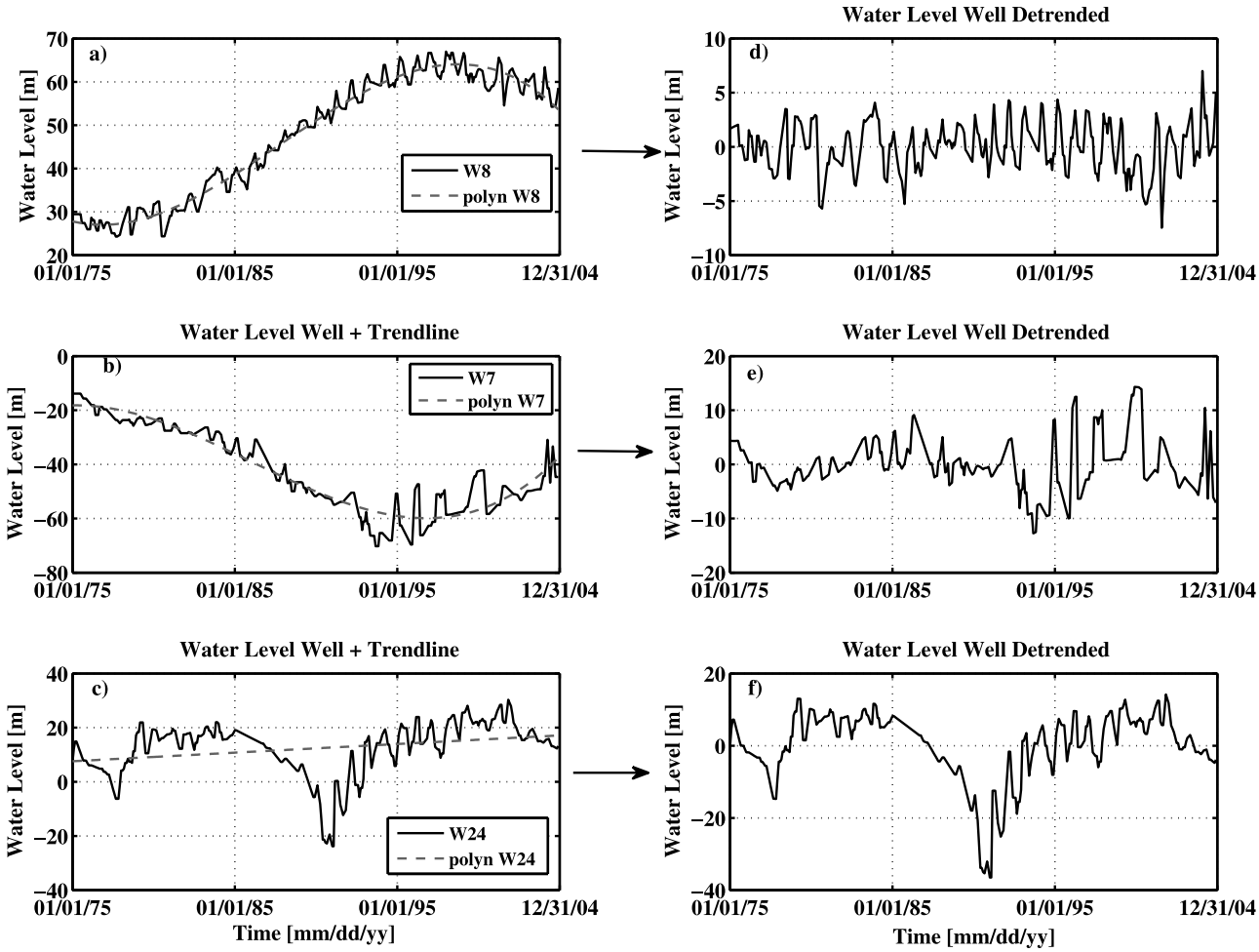

Figure 8. (left) Time series for key wells (a) W8 (group 1), (b) W7 (group 2), and (c) W24 (group 3) and (right) the detrended series for (d) W8, (e) W7, and (f) W24 using a low-order polynomial. Water level time series with the dashed line denote the polynomial trend line.

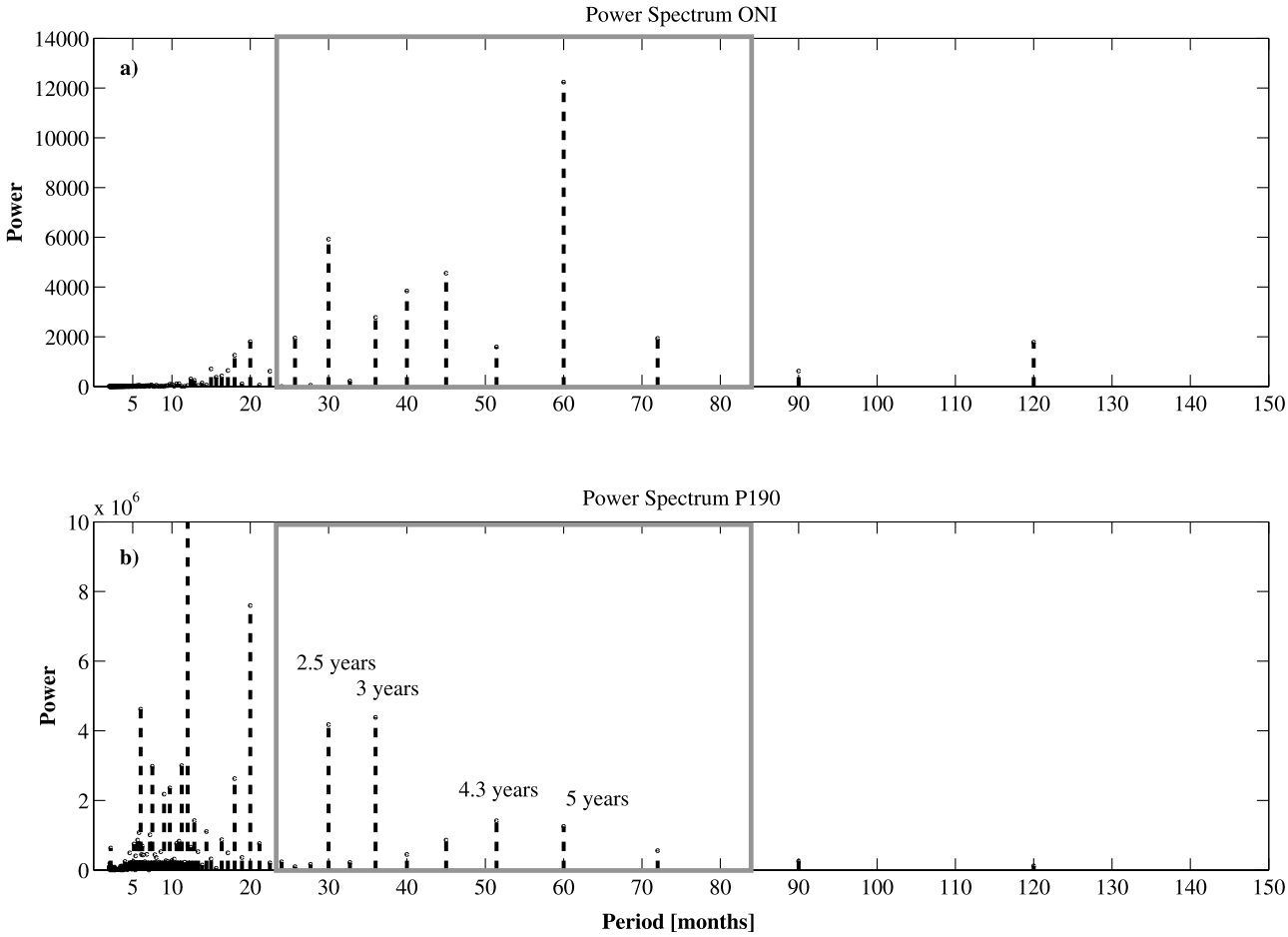

Figure 9. Power spectrum (dashed lines) for (a) monthly ONI time series and (b) precipitation monthly time series for P190. The rectangular box indicates the general range of observed ENSO cycles (2–7 years).

semester of the year in both wells (W7 and W8), most likely due to irrigation demand in the basin. The pumpage records appear to be related with El Niño–Southern Oscillation, but due to the temporal resolution of the wells pumping data (six months period) it is difficult to clearly connect this relationship. For example, during the second half of 1998 the pumping dropped considerably compared with other years in both wells, which is attributed to the El Niño event of 1997–1998. In addition, a trend line was estimated with a low-order polynomial for the raw time series (Figures 8a, 8b, and 8c, groups 1, 2, 3, respectively) and the corresponding detrended time series (Figures 8d, 8e, and 8f, groups 1, 2, 3, respectively).

[30] A large decrease was observed in the groundwater level in well W24 starting in the early 1980s (Figure 7). Well W7 also exhibited decreasing water levels during the same period but the minimum value is observed at later times when compared with Well W24 (Figure 6). Well W8 does not exhibit this behavior (Figure 5). It is observed that all wells, with the exception of W5, W8, W9, W10 (located in East Las Posas) and W17 (located Pleasant Valley), exhibit this pronounced fluctuation during the early 80s. Note that because of their strong correlation, all wells within a group generally show similar behavior, hence all individual well responses are not reported here. To better understand fluctuations in well water levels related to precipitation and El Niño–Southern Oscillation (ONI) signals, the relevant time series are filtered using Fourier analysis.

3.4. Frequency Domain Analysis: Power Spectrum

[31] The linkages between atmospheric modes (ONI indexes) and the periodicity in precipitation and groundwater levels were investigated using the Fourier spectral analysis. Spectral analyses were conducted for monthly data observed over a 30 year period for the ONI index series, the six precipitation series and the 19 well water level series.

[32] Power spectrums for both the El Niño–Southern Oscillation index (ONI) (Figure 9a) and for the precipitation at gauge P190 (Figure 9b) are presented. The time series for the six precipitation gauges selected for this study exhibit a very similar power spectrum, characterized by the highest energy spectrums seen at the annual (12 months) and semiannual (6 month) cycles. Other modes between 2 and 7 years were observed in the precipitation spectrum and coincided with the El Niño–Southern Oscillation (ONI) spectrum, including 2.5 years, 3 years, 4.3 and 5 years (highlighted in Figure 9b).

[33] The power spectrum for the three well groups is represented by the key wells and with other representative wells when differences in the power spectrum are observed within the group. Three different behaviors are observed in group 1, which are represented by W1, key well W8 and W17

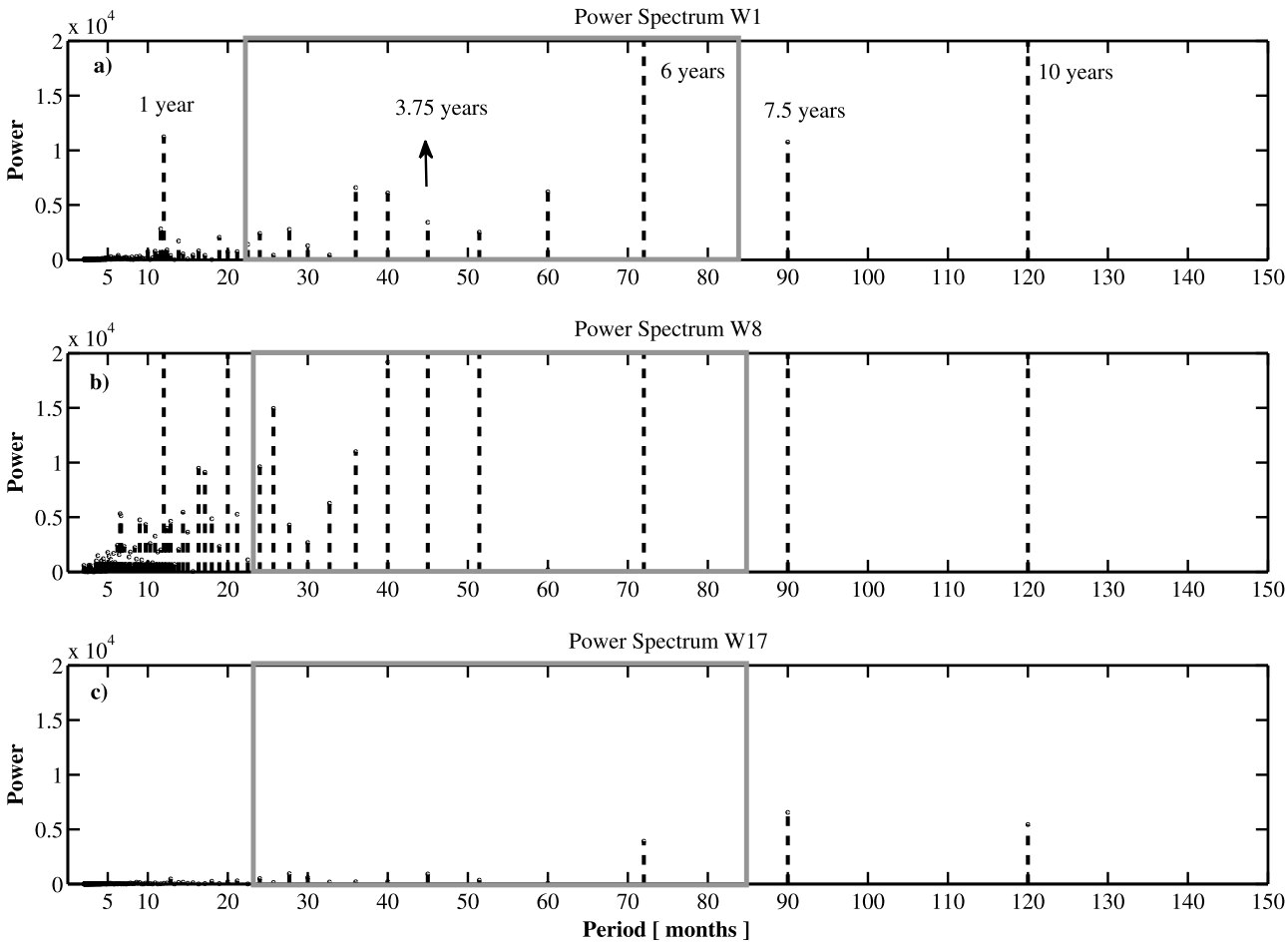

Figure 10. Power spectrum (dashed lines) of water level for (a) W1 (group 1), (b) W8 (group 1), and (c) W17 (group 1). The rectangular box represents the range of observed ENSO cycles (2–7 years).

(Figure 10). Well W1 (Figure 10a) exhibits a strong 6 year, decadal and annual oscillations. This well is located in the Tierra Rejada basin where the aquifer is essentially unconfined and fractured (Tables 1 and 3). Well 1, which is 106 m deep, shows stronger power for low frequencies (large periods), which we hypothesize is related to the travel time of rainfall to the aquifer which is partially filtering the higher frequencies (short periods). The well power spectrum for W8 (Figure 10b, East Las Posas basin) is characterized by a strong decadal mode, strong ONI periodicities and a strong annual cycle. Well W8 is screened in the Fox Canyon aquifer, which is considered confined except near the outcrops (Figure 2). The well depth is 335m, well inside the confined portion of the formation. Well W8 also shows stronger ONI periodicities than W1. A stronger annual cycle and oscillations shorter than 2 years are observed in W8 (group 1). Differences between W1 and W8 can be explained in term of the closer proximity of W8 to the main water course in the watershed [*Luque-Espinar et al.*, 2008]. Well W17 (Figure 10c) is 247 m deep and located in the confined aquifer of Pleasant Valley basin. This well is characterized by stronger periodicities at 6, 7.5 and 10 years. The decrease in the power of the high-frequency components of the signal from this well can be attributed to its relatively deeper screen depth and to the presence of low-permeability confining units. All wells in group 1 exhibited periodicities related with El Niño–Southern Oscillation and with the Pacific Decadal Oscillation.

[34] Group 2 exhibits a similar power spectrum across all wells (Figure 11a, key well W7). The wells of group 2 are located in both the West and East Las Posas basin and are screened within the Fox Canyon and Crimes Canyon aquifers, with an average depth of 390 m. The wells are located in the upper reaches of the watershed, near the outcrops where the aquifers are unconfined. Hence, a more direct connection with the surface (outcrops) and related precipitation forcing is observed in the power spectrum. Similar to the precipitation power spectrum (Figure 9) the average power spectrum of this group is characterized by a strong annual cycle, strong high frequencies related to periods shorter than 1 year, and fluctuations correlated with the ONI signal. This group also exhibits a strong decadal mode.

[35] Group 3 wells exhibit similar power spectrum across all wells (Figure 11b, key well W24). The power spectrum for well W24 is characterized by a strong annual cycle, strong signals with wavelength shorter than 1 year, strong ONI-correlated fluctuations, and a strong decadal mode. Four wells from group 3 are located in the Oxnard basin and one well is located at the boundary with the Pleasant Valley basin. The average well depth is 348 m. Recharge in the Oxnard basin comes from precipitation and infiltration of surface water from the Santa Clara River. As will be shown

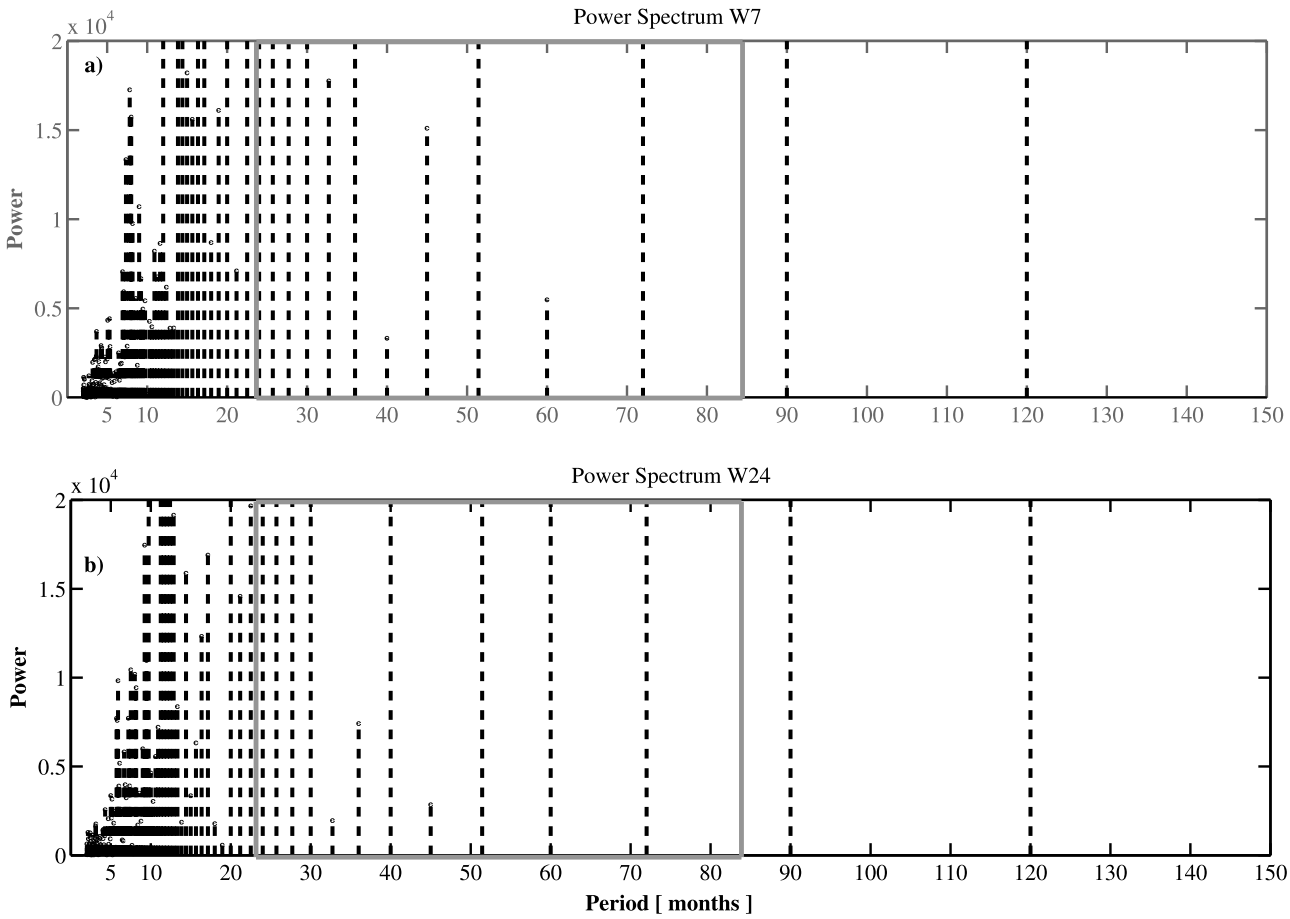

Figure 11. Same as Figure 10 except for (a) W7 (group 2) and (b) W24 (group 3).

later, there is a strong correlation between the wells of this group and the wells located in the Fillmore basin (north of Calleguas watershed). A weak semiannual cycle in the well levels is also present, but with a relatively smaller power. This semiannual signal is most likely related to anthropogenic impacts, and possibly mediated by the travel time of water through the alluvium. The power spectrum exhibits strong periodicities mainly related to the proximity to the main river channel. The behavior in well water fluctuations located in proximity to rivers, characterized with strong ENSO and PDO oscillation, was also observed by *Hanson et al.* [2006] and *Luque-Espinar et al.* [2008].

[36] The variance of the power spectrum for precipitation and each of the key wells is highlighted in Figure 12. The variance of the power spectrum for precipitation data (P190) is presented in Figure 12a. Oscillation between 2 and 7 years explain 11% of the variance. Modes between 0.5 and 2 year explain 82% of the variance, where 50% corresponds with the annual cycle. The decadal mode is weakly represented in the power spectrum with only 0.1% representing the total variance. Well W7 (Figure 12c, group 2) shows a stronger water level correlation with El Niño–Southern Oscillation, as 46% of the variance is represented by modes with periods ranging between 2 and 7 years. For key wells W8 (Figure 12b, group 1) and W24 (Figure 12d, group 3) the power variance of the waves corresponding to ENSO modes represents 31% and 36% of the variance, respectively. The decadal mode justifies 18% of the total variance in W8 (group 1) and 7% in wells W7 (group 2) and W24 (group 3). Modes between 0.5 and 2 years explain 37%, 36% and 32% of the total variance for wells W8 (group 1), W7 (group 2), and W24 (group 3), respectively.

[37] A period of 30 years is relatively short to draw conclusions related to PDO connections and groundwater fluctuations. Unfortunately the majority of wells available within the Calleguas Creek watershed do not have extensive time series. In order to explore the connection of PDO with regional groundwater levels, well and precipitation data for a 56 year period (1950–2006) was obtained from a well (W38) and a precipitation gauge (P96) located in the neighboring Santa Clara watershed, just north of the Calleguas watershed (Figure 1). The well water level time series exhibits an average correlation value of 0.78 with the group 3 wells, while a lower correlation is observed between W38 and groups 1 and 2. Nevertheless, for the purpose of this study, we consider the correlation level with group 3 significant.

[38] Annual average PDO and water level in W38 was calculated for the 1950–2006 period, as well as total yearly precipitation (Figure 13). It is important to clarify that the period 1950–2006 represents roughly two PDO cycles: a cool PDO regime prevailing from 1947 to 1976 and a warm PDO regime from 1977 through (at least) the mid 1990s (http://www.cpc.noaa.gov/). To closer evaluate relationships between precipitation and PDO, we focus on the 1950–1975 period during which the PDO was predominantly negative (average PDO equal to −0.7) and the 1976–1998 period during which PDO was predominantly positive (average PDO equal to 0.6). Annual rainfall averages 496 mm during the

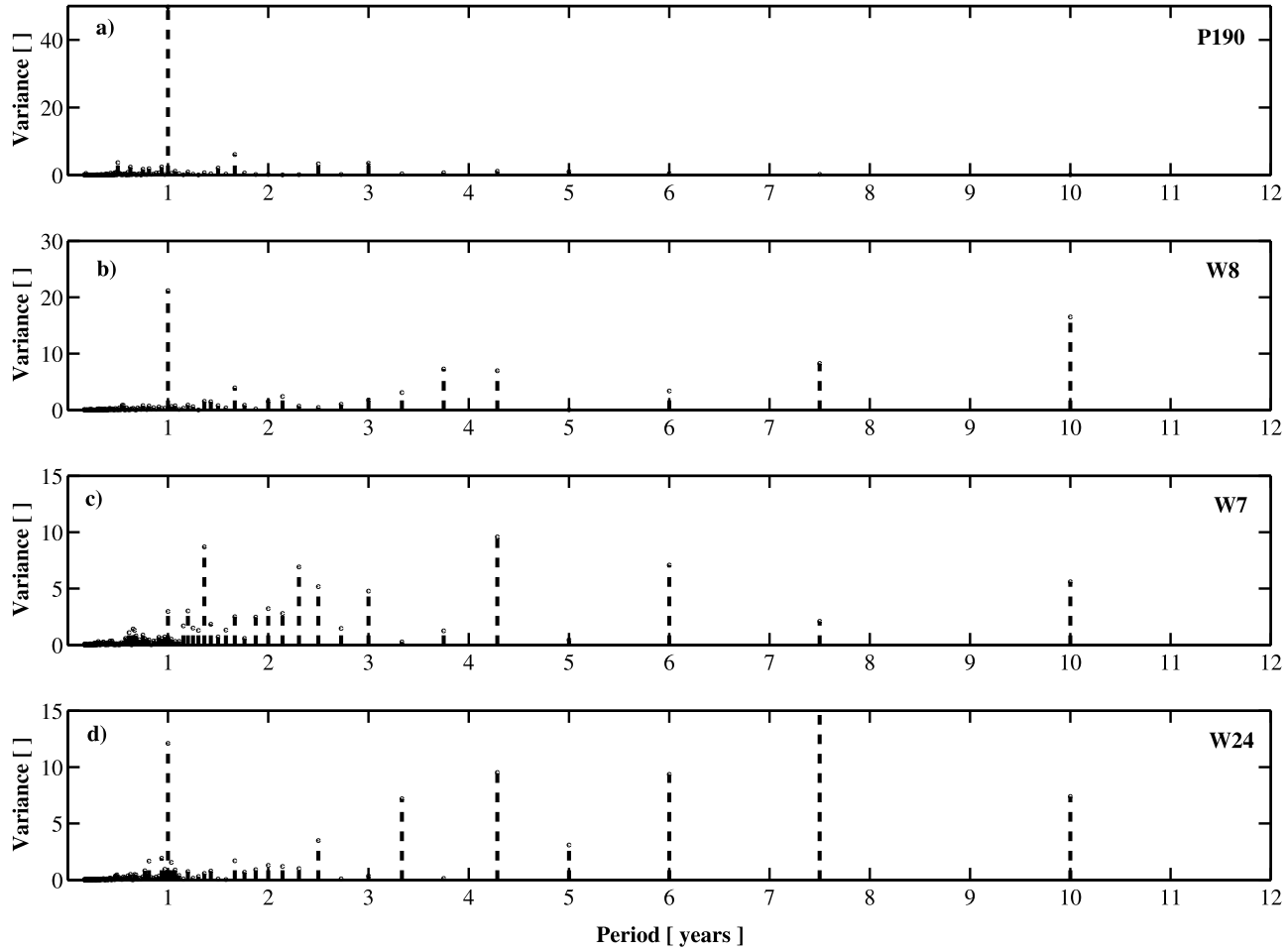

Figure 12. Power spectrum variance of water levels for (a) P190, (b) W8 (group 1), (c) W7 (group 2), and (d) W24 (group 3).

entire period (1950–2006), however, from 1950 to 1976 (negative PDO), rainfall is below average (443 mm; 10% below the period mean), and rainfall from 1977 to 1998 (positive PDO) is above average (566 mm; 12% above the period mean). Precipitation variability also changes during the different periods. The precipitation standard deviation from 1950 to 2006 is 235 mm, while from 1950 to 1975 the standard deviation is lower (197 mm) and from 1976 to 1998 the standard deviation is significantly higher (280 mm). The mean and standard deviation during the negative PDO illustrate that precipitation is below normal and the opposite holds for positive PDO. Looking at the winter periods (defined from December to February) there are also changes in the mean with respect to long-term winter mean. The average winter precipitation during the 1950–1975 period is 11% below the normal winter mean, while winter precipitation is 13% above the winter mean for the 1976–1998 period. The lowest annual PDO index for the period was −1.948 in 1955, which does not correspond with the lowest precipitation in the period; however the precipitation in this year was still 6% below the mean. The highest precipitation during the period was observed in 1983 and corresponds with the second highest PDO index (1.648).

[39] It is observed that the water levels in well W38 are tightly coupled to precipitation variability and, therefore, to fluctuations in the PDO climate signal. It is also observed that the response of groundwater levels may be more impacted by a longer-persistence climate event, such as the PDO, rather than ENSO. Persistent negative PDOs appear to highly impact the groundwater levels. For example, the precipitation was consistently low during the periods 1953–1968, responding to the negative PDO phase. The groundwater level was also significantly decreased during these periods. However, the response of groundwater to persistence rainfall events, in general connected with positive PDO phases, is a noticeable increase in the well water level.

[40] The power spectrum for P96 (Figure 14a) exhibits a very similar power spectrum from the other precipitation gauges in this study (Table 2) with the highest energy spectrum observed at the annual cycle (46% of the total variance). El Niño modes (between 2 and 7 years) represent 11% of the total variance, and PDO, primarily a 14 year mode, represents 1.2% of the total variance. Well W38 (Figure 14b) shows a correlation with ENSO, as 39% of the variance is represented by modes with periods ranging between 2 and 7 years. Ten percent of the variance is represented by a 14 year mode and an 11 year mode represents 5% of the total variance.

4. Summary and Concluding Remarks

[41] Climatologic and hydrologic time series were analyzed in a rapidly urbanizing watershed in southern California

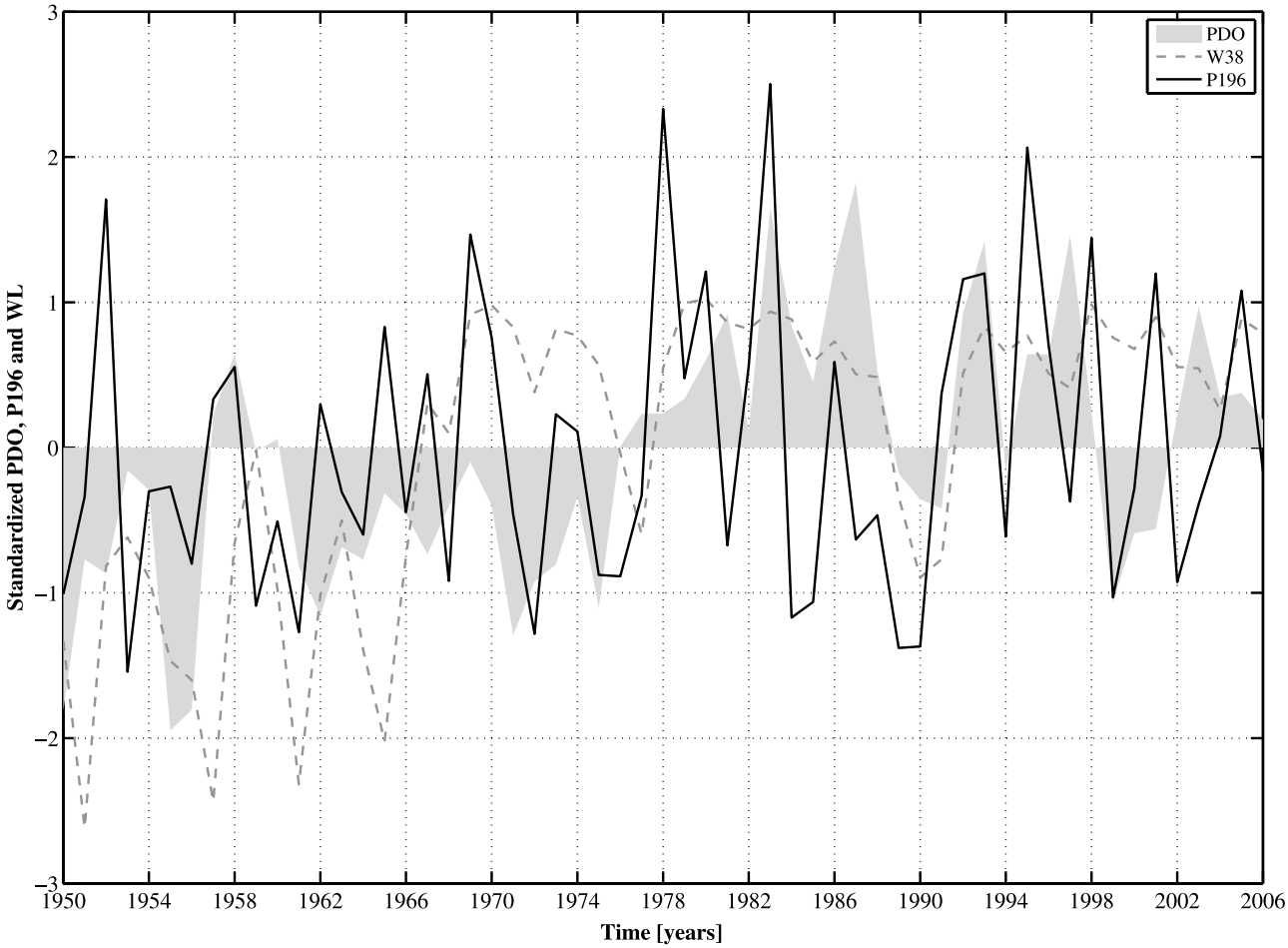

Figure 13. Standardized annual time series of precipitation (black line), water level for W38 (dashed gray line), and Pacific Decadal Oscillation (PDO) (shaded area).

that is heavily dependent on groundwater for agricultural, industrial and municipal water supply. Correlation analysis between well water levels, trend analysis using nonparametric techniques and spectral analyses were conducted for monthly precipitation and groundwater observations over a 30 year period. Connection between climate modes (Niño–Southern Oscillation and Pacific Decadal Oscillation), precipitation and well water level were studied using Fourier analysis. The key findings of the study are summarized as follows.

[42] 1. Wells were grouped into three related subgroups based on a correlation matrix calculated from the water level time series. In general, high correlation is observed between the wells of each group for the period of record (average correlation between groups higher than 0.8). Each group exhibits a significant and distinct trend. Groups of wells located closer to the main river exhibit a significant upward trend, while wells located in the highest part of the watershed exhibit a significant downward trend. Wells located in the floodplain do not appear to exhibit unique trends. The trend analysis provides insight regarding hydrologic (climate) behavior and overall aggregated response of the subbasins. The trend series analysis undertaken in this study can be used for forecasting groundwater levels in different parts of the watershed and ultimately improve time series quality by providing estimates for missing data due to damage of the wells or malfunction of the recording instruments.

[43] 2. The Mann-Kendall identifies a significant upward trend in group 1 wells (closer to the mainstream channels), while group 2 wells (closer to the mountain recharge areas) show a significant downward trend. Group 3 wells (located in the lower plains) exhibit both increasing and decreasing trends. A high percentage of this trend is due to persistence (66–99%) based on the prewhitening analysis.

[44] 3. Groundwater levels and precipitation in Calleguas Creek watershed are responding to regional climate signals, partially coincident with the El Niño–Southern Oscillation modes and the Pacific Decadal Oscillation. The spectral analysis presents significant common periodicities between 2.0 and 7.0 years and shows a strong linkage with the ENSO signal. Results also showed that water levels responded to longer-term precipitation variability and therefore to fluctuations in the PDO climate signal. It is also observed that the response of groundwater levels is highly impacted by longer-persistence climate events such as the Pacific Decadal Oscillation.

[45] 4. Spectral analysis improves our understanding of both properties and processes in surface-groundwater systems. The spectral analysis reveals the portion of the time series structure that cannot be observed easily in the time domain, and can be used effectively to better describe the

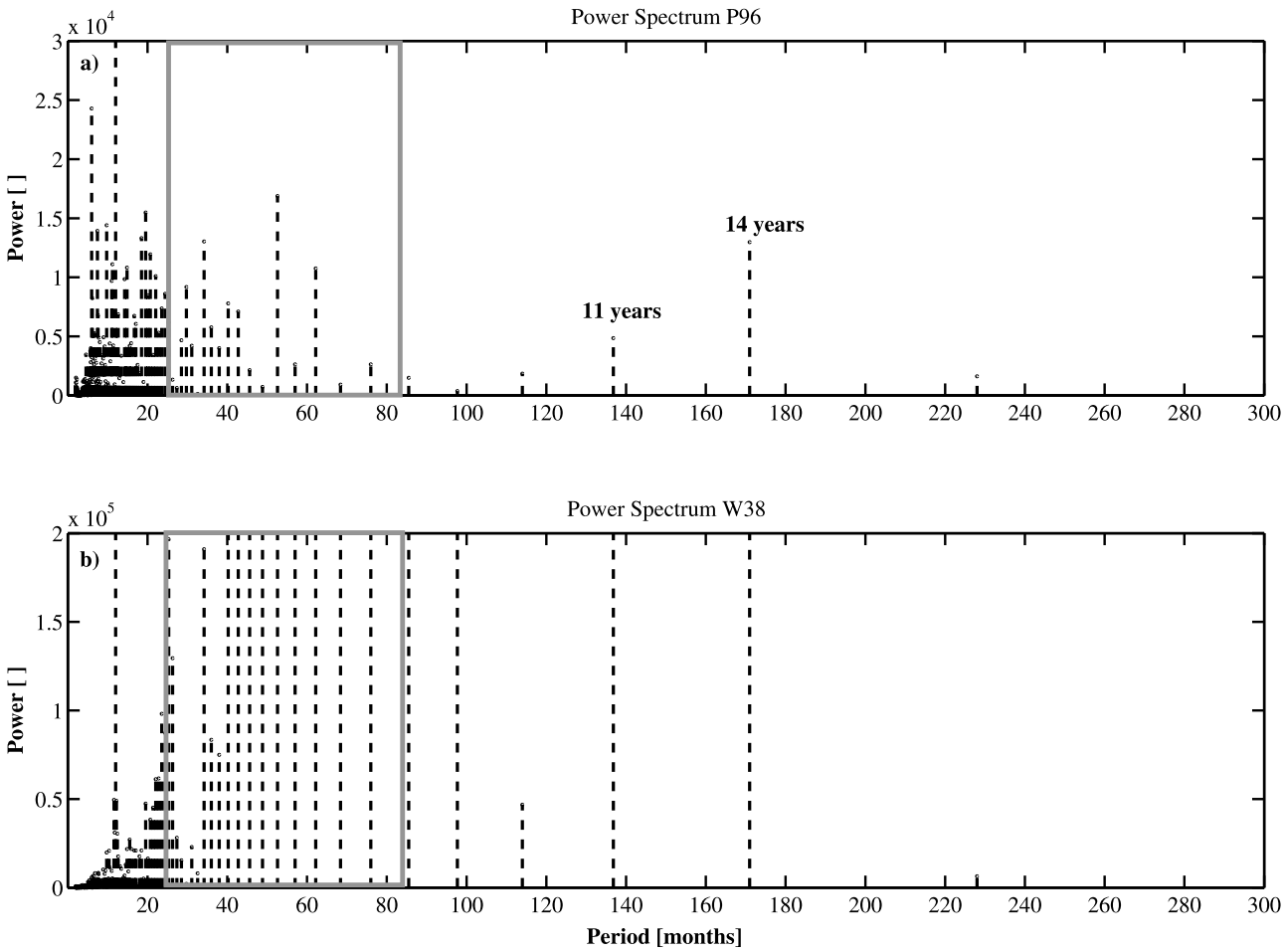

Figure 14. Power spectrum (dashed lines) for (a) monthly time series of precipitation at gauge P96 and (b) water levels for W38. The darker rectangle represents the range of ENSO cycles (2–7 years).

relationships between different variables. In this study, spectral was successfully applied to highlight the linkages between climate-surface-aquifer water interactions and provided a powerful tool to understand the physical connections between surface and subsurface water bodies. Results highlight that the level of impact of climate oscillations on groundwater systems depends on the aquifer characteristics (confined or unconfined), spatial well locations and screen depth, and particularly, direct connections with the surface (well close to the aquifer outcrops or water courses).

[46] We conclude our analysis with the following observations. Parts of eastern Ventura County in the Calleguas Creek Watershed are highly dependent on imported water from the State Water Project. Reducing dependence on imported water for this area and other southern California regions is obviously a challenge for watersheds managers and planners. Calleguas Creek Municipal Water District (CCMWD) operates a groundwater conjunctive use project (North Las Posas) within the study watershed. Water typically stored in the aquifers during the winter months becomes a strategic asset during the summer period, when surface water supplies are low and demands are high. Better understanding of the spatial and temporal variability in groundwater levels within a large aquifer system and related linkages with climate variability is a critical component for improving water supply reliability for local and regional managing water districts, including CCMWD. In addition, the identification of well correlations and cycles can be used to help develop models for artificial recharge within groundwater systems. Results from this study can also help in developing policies and regulations for the Calleguas Creek watershed as well as other groundwater basins across the southern California region.

[47] **Acknowledgments.** Financial support for this work was provided by a grant from the Calleguas Creek Municipal Water District. This support is greatly appreciated. Ricardo Mantilla, at the University of Iowa, also provided valuable discussion and insight.

References

Ahmadi, S., and A. Sedghamiz (2007), Geostatistical analysis of spatial and temporal variations of groundwater level, *Environ. Monit. Assess.*, *129*(1–3), 277–294, doi:10.1007/s10661-006-9361-z.

Alley, W. M., T. E. Reilly, and O. L. Franke (1999), *Sustainability of groundwater resources*, *U.S. Geol. Surv. Circ.*, *1186*.

Andrade, E. R., and W. D. Sellers (1988), El Niño and its effect on precipitation in Arizona and western New Mexico, *J. Climatol.*, *8*, 403–410, doi:10.1002/joc.3370080407.

Bove, M. (1998), Effect of El Nino on US landfalling hurricanes, *Bull. Am. Meteorol. Soc.*, *79*(11), 2477–2482, doi:10.1175/1520-0477(1998)079<2477:EOENOO>2.0.CO;2.

Box, G. E. P., and G. M. Jenkins (1976), *Time Series Analysis: Forecasting and Control*, Holden Day, San Francisco, Calif.

Burke, J. J., and M. Moench (2000), *Groundwater and Society: Resources, Tensions, Opportunities*, 170 pp., U.N., New York.

California Department of Water Resources (CDWR) (2003), California's groundwater. Update of Bulletin 118, Sacramento, Calif.

California Regional Water Quality Control Board (1994), Basin plan for the coastal watersheds of Los Angeles and Ventura counties, Los Angeles, Calif.

Calleguas Creek Watershed Management Plan Committee (CCWMP) (2004), Calleguas Creek watershed management plan, phase 1, November 10, 2004, Thousand Oaks, Calif.

Cayan, D. R. (1996), Interannual climate variability and snowpack in the western United States, *J. Clim.*, *9*, 928–948, doi:10.1175/1520-0442(1996)009<0928:ICVASI>2.0.CO;2.

Cayan, D. R., M. D. Dettinger, E. F. Diaz, and N. E. Graham (1998), Decadal variability of precipitation over western North America, *J. Clim.*, *11*, 3148–3166, doi:10.1175/1520-0442(1998)011<3148:DVOPOW>2.0.CO;2.

Cayan, D. R., K. T. Redmond, and L. G. Riddle (1999), ENSO and hydrologic extremes in the western United States, *J. Clim.*, *12*, 2881–2893, doi:10.1175/1520-0442(1999)012<2881:EAHEIT>2.0.CO;2.

Chambers, J. M., W. S. Cleveland, B. Kleiner, and P. A. Tukey (1983), *Graphical Methods for Data Analysis*, 395 pp., Duxbury, Boston, Mass.

Chen, Z., S. E. Grasby, and K. G. Osadetz (2004), Relation between climate variability and groundwater levels in the upper carbonate aquifer, southern Manitoba, Canada, *J. Hydrol.*, *290*, 43–62, doi:10.1016/j.jhydrol.2003.11.029.

Christensen, S. N., W. A. Wood, N. Voisin, P. D. Lettenmaier, and N. R. Palmer (2004), The effects of climate change on the hydrology and water resources of the Colorado River Basin, *Clim. Change*, *62*(1–3), 337–363, doi:10.1023/B:CLIM.0000013684.13621.1f.

Cook, A. R., and J. T. Schaefer (2008), The relation of El Nino–Southern Oscillation (ENSO) to winter tornado outbreaks, *Mon. Weather Rev.*, *136*, 3121–3137, doi:10.1175/2007MWR2171.1.

Dettinger, M. D., D. R. Cayan, H. F. Diaz, and D. M. Meko (1998), North-south precipitation patterns in western North America on interannual-to-decadal timescales, *J. Clim.*, *11*, 3095–3111, doi:10.1175/1520-0442(1998)011<3095:NSPPIW>2.0.CO;2.

Diaz, H. F., and R. S. Pulwarty (1994), An analysis of the time scales of variability in centuries-long ENSO-sensitive records, *Clim. Change*, *26*, 317–342, doi:10.1007/BF01092422.

Douglas, E. M., R. M. Vogel, and C. N. Kroll (2000), Trends in floods and low flows in the United States: Impact of spatial correlation, *J. Hydrol.*, *240*, 90–105.

Dracup, J. A., and D. R. Kendall (1989), Floods and droughts, in *Climate Change and U.S. Water Resources*, edited by P. E. Waggoner and R. Revelle, chap. 11, pp. 243–268, John Wiley, New York.

Echer, M. P. S., E. Echer, N. R. Rigozo, D. J. R. Nordemann, and A. Prestes (2008), Wavelet analysis of a centennial (1895–1994) southern Brazil rainfall series, *Clim. Change*, *87*(3–4), 489–497, doi:10.1007/s10584-007-9296-6.

Faunt, C. C. (Ed.) (2009), Groundwater availability of the Central Valley Aquifer, California, *U.S. Geol. Surv. Prof. Pap.*, *1766*, 225 pp. (Available at http://pubs.usgs.gov/pp/1766/)

Fleming, S. W., A. M. Lavenue, A. H. Aly, and A. Adams (2002), Practical applications of spectral analysis to hydrologic time series, *Hydrol. Processes*, *16*(2), 565–574, doi:10.1002/hyp.523.

Fox Canyon Groundwater Management Agency (2006), Fox Canyon groundwater management plan, public review draft, Ventura, Calif.

Fraedrich, K., and H. Boettger (1978), A wave number-frequency analysis of the 500 mb geopotential lat50N, *J. Atmos. Sci.*, *35*, 745–750, doi:10.1175/1520-0469(1978)035<0745:AWFAOT>2.0.CO;2.

García, N. O., L. Gimeno, L. de la Torre, R. Nieto, and J. A. Añel (2005), North Atlantic Oscillation (NAO) and precipitation in Galicia (Spain), *Atmosfera*, *18*, 25–32.

Glantz, M. H. (2001), *Currents of Change: Impacts of El Niño and La Niña on Climate and Society*, 2nd ed., Cambridge Univ. Press, Cambridge, U. K.

Gleick, P. H. (1985), Regional hydrologic impacts of global climate changes, paper presented at International Research and Development Conference Arid Lands: Today and Tomorrow, Off. of Arid Land Stud., Univ. of Ariz., Tucson.

Gleick, P. H. (2003), Freshwater resources: Soft-path solutions for the 21st century, *Science*, *302*, 1524–1528, doi:10.1126/science.1089967.

Glennon, R. (2002), *Water Follies: Groundwater Pumping and the Fate of America's Fresh Waters*, Island, Washington, D. C.

Guirguis, K. J., and R. Avissar (2008), Analysis of precipitation variability, persistence, and observational data uncertainty in the western United States, *J. Hydrometeorol.*, *9*(5), 843–865, doi:10.1175/2008JHM972.1.

Gurdak, J. J., R. T. Hanson, P. B. McMahon, B. W. Bruce, J. E. McCray, G. D. Thyne, and R. C. Reedy (2007), Climate variability controls on unsaturated-zone water and chemical movement, High Plains aquifer, *Vadose Zone J.*, *6*, 533–547, doi:10.2136/vzj2006.0087.

Hamlet, A. F., and D. P. Lettenmaier (1999), Effects of climate change on hydrology and water resources of the Columbia River Basin, *J. Am. Water Resour. Assoc.*, *35*, 1597–1623, doi:10.1111/j.1752-1688.1999.tb04240.x.

Hanson, R. T., and M. D. Dettinger (2005), Ground-water/surface-water responses to global climate simulations, Santa Clara–Calleguas Basin, Ventura County, California, 1950–93, *J. Am. Water Resour. Assoc.*, *41*(3), 517–536, doi:10.1111/j.1752-1688.2005.tb03752.x.

Hanson, R. T., P. Martin, and K. M. Koczot (2003), Simulation of ground-water/surface-water flow in the Santa Clara–Calleguas basin, California, *U.S. Geol. Surv. Water Resour. Invest. Rep., 02-4136*, 214 pp. (Available at http://water.usgs.gov/pubs/wri/wri024136/text.html)

Hanson, R. T., M. W. Newhouse, and M. D. Dettinger (2004), A methodology to assess relations between climate variability and variations in hydrologic time series in the southwestern United States, *J. Hydrol.*, *287*, 252–269, doi:10.1016/j.jhydrol.2003.10.006.

Hanson, R. T., M. D. Dettinger, and M. W. Newhouse (2006), Relations between climate variability and hydrologic time series from four alluvial basins across the southwestern United States, *Hydrogeol. J.*, *14*, 1122–1146, doi:10.1007/s10040-006-0067-7.

Hidalgo, H. G., and J. A. Dracup (2003), ENSO and PDO effects on hydroclimatic variations of the Upper Colorado River Basin, *J. Hydrometeorol.*, *4*(1), 5–23, doi:10.1175/1525-7541(2003)004<0005:EAPEOH>2.0.CO;2.

Hogan, J. F., F. M. Phillips, and B. R. Scanlon (2004), *Groundwater Recharge in a Desert Environment: The Southwestern United States*, *Water Sci. Appl. Ser.*, vol. 9, 294 pp., AGU, Washington, D. C.

Hoque, M. A., M. M. Hoque, and K. M. Ahmed (2007), Declining groundwater level and aquifer dewatering in Dhaka metropolitan area, Bangladesh: Causes and quantification, *Hydrogeol. J.*, *15*, 1523–1534, doi:10.1007/s10040-007-0226-5.

Hutson, S. S., N. L. Barber, J. F. Kenny, K. S. Linsey, D. S. Lumia, and M. A. Maupin (2004), Estimated use of water in the United States in 2000, *U.S. Geol. Surv. Circ.*, *1268*, 46 p.

Intergovernmental Panel on Climate Change (IPCC) (2001), *Climate Change 2001: The Scientific Basis*, edited by J. T. Houghton et al., 881 pp., Cambridge Univ. Press, Cambridge, U. K.

Kang, S., and H. Lin (2007), Wavelet analysis of hydrological and water quality signals in an agricultural watershed, *J. Hydrol.*, *338*, 1–14.

Kao, S. K. (1968), Governing equations and spectra for atmospheric motion and transports in frequency wave-number space, *J. Atmos. Sci.*, *25*(1), 32–38, doi:10.1175/1520-0469(1968)025<0032:GEASFA>2.0.CO;2.

Kendall, M., and J. D. Gibbons (1990), *Rank Correlation Methods*, 5th ed., 272 pp., Oxford Univ. Press, Oxford, U. K.

Khaliq, M. N., T. B. M. J. Ouarda, P. Gachon, and L. Sushama (2008), Temporal evolution of low-flow regimes in Canadian rivers, *Water Resour. Res.*, *44*, W08436, doi:10.1029/2007WR006132.

Koutsoyiannis, D., and A. Montanari (2007), Statistical analysis of hydroclimatic time series: Uncertainty and insights, *Water Resour. Res.*, *43*, W05429, doi:10.1029/2006WR005592.

Labat, D., J. Ronchail, J. Callede, J. L. Guyot, E. De Oliveira, and W. Guimaraes (2004), Wavelet analysis of Amazon hydrological regime variability, *Geophys. Res. Lett.*, *31*, L02501, doi:10.1029/2003GL018741.

Lines, G. C. (1996), Ground-water and surface-water relations along the Mojave River, southern California, *U.S. Geol. Surv. Water Resour. Invest. Rep.*, *95-4189*, 43 pp.

Lines, G. C., and T. W. Bilhorn (1996), Riparian vegetation and its water use during 1995 along the Mojave River, southern California, *U.S. Geol. Surv. Water Resour. Invest. Rep.*, *96-4241*, 10 pp.

Luque-Espinar, J. A., M. Chica-olmo, E. Pardo-igúzquiza, and M. J. García-soldado (2008), Influence of climatological cycles on hydraulic heads across a Spanish aquifer, *J. Hydrol.*, *354*, 33–52, doi:10.1016/j.jhydrol.2008.02.014.

MacDonald, G. M., and R. A. Case (2005), Variations in the Pacific Decadal Oscillation over the past millennium, *Geophys. Res. Lett.*, *32*, L08703, doi:10.1029/2005GL022478.

Mann, M. E., and J. Park (1994), Global scale modes of surface temperature variability on interannual to century time scales, *J. Geophys. Res.*, *99*, 25,819–25,833, doi:10.1029/94JD02396.

Mantua, N., and H. Steven (2002), The Pacific Decadal Oscillation, *J. Oceanogr.*, *58*(1), 35–44, doi:10.1023/A:1015820616384.

Mantua, N. J., S. R. Hare, J. M. Wallace, and R. C. Francis (1997), A Pacific decadal climate oscillation with impacts on salmon production, *Bull. Am. Meteorol. Soc.*, *78*, 1069–1079, doi:10.1175/1520-0477(1997)078<1069:APICOW>2.0.CO;2.

Mayer, T. D., and R. D. Congdon (2008), Evaluating climate variability and pumping effects in statistical analyses, *Ground Water*, *46*(2), 212–227, doi:10.1111/j.1745-6584.2007.00381.x.

Minobe, S. (1997), A 50–70 year oscillation over the North Pacific and North America, *Geophys. Res. Lett.*, *24*, 683–686, doi:10.1029/97GL00504.

Mo, K. C., and R. W. Higgins (1998), Tropical influences on California precipitation, *J. Clim.*, *11*, 412–430, doi:10.1175/1520-0442(1998)011<0412:TIOCP>2.0.CO;2.

Morales, J. E., and G. Poveda (2009), Diurnally driven scaling properties of Amazonian rainfall fields: Fourier spectra and order-*q* statistical moments, *J. Geophys. Res.*, *114*, D11104, doi:10.1029/2008JD011281.

Nash, L. L., and P. Gleick (1993), The Colorado River Basin and climate change: The sensitivity of streamflow and water supply to variations in temperature and precipitation, *Rep. EPA 230-R-93-009*, Environ. Prot. Agency, Washington, D. C.

Newland, D. E. (1993), *An Introduction to Random Vibrations, Spectral and Wavelet Analysis*, 477 pp., Addison Wesley Longman, Essex, U. K.

Nigam, S., M. Barlow, and E. H. Berbery (1999), Analysis links Pacific decadal variability to drought and streamflow in the United States, *Eos Trans. AGU*, *80*(51), 621, doi:10.1029/99EO00412.

Padmanabhan, G., and A. R. Rao (1988), Maximum entropy spectral analysis of hydrologic data, *Water Resour. Res.*, *24*(9), 1519–1533, doi:10.1029/WR024i009p01519.

Poveda, G., W. Rojas, M. L. Quiñones, I. D. Vélez, R. Mantilla, and D. Ruiz (2001), Coupling between annual and ENSO timescales in the malaria-climate association in Colombia, *Environ. Health Perspect.*, *109*(5), 489–493, doi:10.2307/3454707.

Rasmussen, E. M. (1984), El Niño: The ocean/atmosphere connection, *Oceanus*, *27*, 5–12.

Salas, J. D., J. W. Delleur, V. Yevjevich, and W. L. Lane (1988), *Applied Modeling of Hydrologic Time Series*, Water Resour. Publ., Littleton, Colo.

Scanlon, B. R., K. E. Keese, A. L. Flint, L. E. Flint, C. B. Gaye, M. Edmunds, and I. Simmers (2006), Global synthesis of groundwater recharge in semi-arid and arid regions, *Hydrol. Processes*, *20*, 3335–3370, doi:10.1002/hyp.6335.

Schonher, T., and S. E. Nicholson (1989), The relationship between California rainfall and ENSO events, *J. Clim.*, *2*(11), 1258–1269, doi:10.1175/1520-0442(1989)002<1258:TRBCRA>2.0.CO;2.

Simpson, H. J., and D. C. Colodner (1999), Arizona precipitation response to the Southern Oscillation: A potential water management tool, *Water Resour. Res.*, *35*(12), 3761–3769, doi:10.1029/1999WR900199.

Smith, L. C., D. L. Turcott, and B. L. Isacks (1998), Stream flow characterization and feature detection using a discrete wavelet transform, *Hydrol. Processes*, *12*, 233–249, doi:10.1002/(SICI)1099-1085(199802)12:2<233::AID-HYP573>3.0.CO;2-3.

Smith, T. M., R. W. Reynolds, T. C. Peterson, and J. Lawrimore (2008), Improvements to NOAA's historical merged land-ocean surface temperature analysis (1880–2006), *J. Clim.*, *21*, 2283–2296, doi:10.1175/2007JCLI2100.1.

Stamos, C. L., P. Martin, T. Nishikawa, and B. F. Cox (2001), Simulation of ground-water flow in the Mojave River Basin, California, *U.S. Geol. Surv. Water Resour. Invest. Rep.*, *01-4002*, 129 pp.

Thomas, B. E. (2007), Climatic fluctuations and forecasting of streamflow in the Lower Colorado River Basin, *J. Am. Water Resour. Assoc.*, *43*(6), 1550–1569.

Torrence, C., and G. P. Compo (1998), A practical guide to wavelet analysis, *Bull. Am. Meteorol. Soc.*, *79*, 61–78, doi:10.1175/1520-0477(1998)079<0061:APGTWA>2.0.CO;2.

Trenberth, K., and J. M. Karon (2000), The Southern Oscillation revisited: Sea level pressures, surface temperatures, and precipitation, *J. Clim.*, *13*(24), 4358–4365, doi:10.1175/1520-0442(2000)013<4358:TSORSL>2.0.CO;2.

Venencio, M. V., and N. O. Garcia (1998), On the droughts in the 'Pampa Humeda' (Argentina) and its relations with alternative water resources, paper presented at 78th Annual Meeting, Am. Meteorol. Soc., Phoenix, Ariz.

Voisin, N., A. F. Hamlet, L. P. Graham, D. W. Pierce, T. P. Barnett, and D. P. Lettenmaier (2006), The role of climate forecasts in western U.S. power planning, *J. Appl. Meteorol.*, *45*(5), 653–673, doi:10.1175/JAM2361.1.

Welch, P. D. (1967), The use of fast Fourier transform for the estimation of power spectra: A method based on time averaging over short, modified periodograms, *IEEE Trans. Audio Electroacoust.*, *15*(2), 70–73, doi:10.1109/TAU.1967.1161901.

von Storch, H. (1995), Misuses of statistical analysis in climate research, in *Analysis of Climate Variability: Applications of Statistical Techniques*, edited by H. von Storch and A. Navarra, pp. 11–26, Springer, New York.

Yue, S., P. Pilon, and B. Phinney (2003), Canadian streamflow trend detection: Impacts of serial and cross correlation, *Hydrol. Sci. J.*, *48*(1), 51–63, doi:10.1623/hysj.48.1.51.43478.

Zhang, Q., C. Xu, T. Jiang, and Y. Wu (2007), Possible influence of ENSO on annual maximum streamflow of the Yangtze River, China, *J. Hydrol.*, *333*, 265–274, doi:10.1016/j.jhydrol.2006.08.010.

Zhang, Y., J. M. Wallace, and D. S. Battisti (1997), ENSO-like interdecadal variability, *J. Clim.*, *10*, 1004–1020, doi:10.1175/1520-0442(1997)010<1004:ELIV>2.0.CO;2.

J. Barco, M. Girotto, and T. S. Hogue, Department of Civil and Environmental Engineering, University of California, 5731F Boelter Hall, Los Angeles, CA 90095-1593, USA. (thogue@seas.ucla.edu)

D. R. Kendall, Calleguas Municipal Water District, 2100 Olsen Rd., Thousand Oaks, CA 91362, USA.

M. Putti, Department of Mathematical Methods and Models for Scientific Applications, University of Padua, via Belzoni 7, I-35131 Padova, Italy.